MOX-Report No. 48/2025

On the inf-sup condition for Hierarchical Model reduction of the Stokes problem

Temellini, E.; Ballarin, F.; Chacon Rebollo, T.; Perotto, S.

MOX, Dipartimento di Matematica
Politecnico di Milano, Via Bonardi 9 - 20133 Milano (Italy)

mox-dmat@polimi.it https://mox.polimi.it

On the inf-sup condition for Hierarchical Model reduction of the Stokes problem

Erika Temellini[1], Francesco Ballarin[2,3],
Tomás Chacón Rebollo[4], Simona Perotto[1]

[1] MOX – Department of Mathematics
Politecnico di Milano
Piazza L. da Vinci, 32, 20133 Milano, Italy
{erika.temellini, simona.perotto}@polimi.it

2 Department of Mathematics and Physics
Università Cattolica del Sacro Cuore
Via Garzetta, 48, 25133, Brescia, Italy
francesco.ballarin@unicatt.it

3 Department of Mathematics for Economic, Financial and Actuarial Sciences
Università Cattolica del Sacro Cuore
Via Necchi, 9, 20123, Milano, Italy

4 Departamento de Ecuaciones Diferenciales y Analisis Numerico & IMUS
Universidad de Sevilla
Apartado de Correos, 1160, 41080, Sevilla, Spain
chacon@us.es

Abstract

Hierarchical Model Reduction is an effective Reduced Order Modelling technique for problems defined on elongated, pipe-like domains. It is particularly suitable when a dominant dynamics is aligned with the longitudinal direction, while transverse effects are locally significant but spatially limited.
When applied to two-field problems such as the Stokes equations, a main challenge is to ensure the stability of the reduced formulation, particularly the inf-sup condition for pressure discretization. In this work, we provide a rigorous analysis showing that the inf-sup condition holds whenever the number of velocity modes is at least equal to the number of pressure modes, thereby extending previous heuristic approaches. The proof exploits the separation of variables in HiMod and is valid for pipe-like domains under some geometric assumptions. Numerical assessment confirms the theoretical findings, providing a solid foundation for stable and efficient HiMod reduction in incompressible flow problems.

Keywords Stokes equations; hierarchical model reduction; inf-sup condition; educated modal expansion; finite elements.

1 Introduction

Reduced Order Modelling (ROM) has become an essential tool in computational science, offering a practical alternative to high-fidelity models. These often involve millions of variables, particularly for large-scale problems governed by partial differential equations, making traditional numerical approaches computationally prohibitive. This is the case, for instance, of contexts requiring repeated evaluations of the governing equations such as in optimization, control, inverse analysis, uncertainty quantification, and real-time or multi-query scenarios.

ROM techniques aim to replace the full-order model with a surrogate that captures the dominant features of the problem at hand, while drastically reducing the associated number of variables. This approach leads, on average, to a significant reduction in computational cost and time. The resulting trade-off between efficiency and accuracy has proven crucial across a broad spectrum of application domains, including fluid and structural mechanics, electromagnetics, thermal sciences, biomedical simulations, energy systems, geophysics, and acoustics. In these fields, ROM enables virtual prototyping of scenarios that would otherwise be numerically intractable.

Among the most widely adopted ROM techniques are Proper Orthogonal Decomposition (POD), Proper Generalized Decomposition (PGD), Reduced Basis (RB) Methods, Galerkin projection-based approaches, and Hierarchical Model (HiMod) reduction. A comprehensive introduction to the theoretical foundations and applications of ROM can be found in [1, 2, 3, 4, 5, 6, 7].

This work is devoted to HiMod reduction, a ROM technique developed to efficiently tackle problems exhibiting a dominant direction of propagation, while still accounting for secondary transverse dynamics. Such configurations frequently occur in elongated, pipe-like domains, where one dimension governs the main behavior of the system.

The core idea behind HiMod is to exploit a separation of variables approach, using distinct approximation strategies along the dominant and transverse directions. In the early development of HiMod reduction, a classical finite element (FE) discretization was adopted along the dominant direction, while a standard sinusoidal modal expansion was employed to account for transverse dynamics [8, 9]. This results in a dimensionality reduction that reformulates the full model as a system of coupled one-dimensional equations, regardless of the dimensionality of the original problem. As a consequence, HiMod reduction has been successfully applied to several real-life problems, such as linear acoustics [10], advection-diffusion reaction phenomena [11, 8, 12, 13, 9, 14], blood flow modeling [15, 16] also in patient-specific artery segments [17] and electromagnetic framework [18].

In recent advancements, the FE approximation has been replaced by isogeometric analysis, which offers great flexibility in representing geometrically complex domains and challenging dynamics [19, 17]. As for the choice of the modal basis, the most effective and versatile strategy so far relies on the so-called educated modal basis, built from the eigenfunctions of a Sturm–Liouville problem [11]. This choice allows for an explicit incorporation of the boundary conditions prescribed along the transverse boundaries, thereby improving the accuracy and adaptability of the reduced model. It is also possible to vary the number of modes used to describe the transverse dynamics. This leads to the concepts of

model hierarchy and adaptivity, where the number of modal functions is adjusted locally (i.e., more modes are used in regions with rich dynamics while fewer where the behavior is smoother), coherently with the local complexity of the solution. In particular, the number of modal functions can be tuned either a priori, based on preliminary insights into the expected behavior of the system [8, 9, 20, 21], or automatically, by relying on an a posteriori modeling error analysis [22, 23, 24]. While selecting the number of modes is certainly an important aspect, it can be considered somewhat optional in certain contexts (e.g., for elliptic problems) where, in the worst case, the simulation remains feasible albeit less efficient. However, in the case of two-field problems, such as the Stokes equations studied in this work, this choice becomes essential to ensure both accuracy and stability of the reduced model. So far, an empirical strategy has been adopted, based on a heuristic criterion that assumes a specific scaling between the number of modal functions used to approximate the transverse dynamics of velocity and pressure, respectively [25, 15, 17, 26]. In all these references, a stable pressure field is computed, although pressure approximation remains the most challenging component.

The goal of this work is to provide a rigorous theoretical analysis to guarantee the stability of the HiMod pressure discretization in terms of the inf-sup condition. We prove that this condition is satisfied whenever the number of velocity modes is equal to or greater than the number of pressure modes. This result extends the current state-of-the-art by allowing a broader range of admissible combinations for the two modal indices.
The proof is based on constructing a velocity field whose divergence reproduces a given pressure profile. This is achieved by solving a Cauchy problem for a system of ordinary differential equations governing the velocity modal coefficients, which admits a unique solution. Thanks to the separation of variables underlying the HiMod formulation, the problem is restricted to the dominant (longitudinal) direction only.
The analysis is carried out on a general class of pipe-like domains that can be mapped smoothly to a reference configuration. To ensure the validity of the theoretical results, we assume some geometric constraints on this mapping, allowing only small deformations from a rectangular configuration.

The paper is structured as follows. Section 2 details the HiMod discretization for the Stokes problem. In Sec. 3, we present a set of preliminary results that are instrumental for proving the well-posedness of the HiMod discretization for the Stokes problem, which is the focus of the subsequent section. In Sec. 5, we validate the theoretical findings through numerical tests across different geometries. In particular, we examine the optimality of the condition on the number of modal functions required to satisfy the inf-sup stability, comparing it against the heuristic strategy currently adopted in the literature. Moreover, we verify the key geometric assumptions underlying the proposed inf-sup analysis, particularly those related to the admissible shapes of the computational domain. Finally, concluding remarks are provided in the last section.

2 HiMod semidiscrete formulation of the Stokes problem

In this work, we focus on the steady Stokes equations, modeling an incompressible viscous flow in a domain $\Omega \subset \mathbb{R}^2$, with boundary $\partial\Omega$, namely

$$\begin{cases} -\nu\,\Delta\mathbf{u}(\mathbf{z}) + \nabla p(\mathbf{z}) = \mathbf{f}(\mathbf{z}) & \text{in } \Omega \\ \nabla\cdot\mathbf{u}(\mathbf{z}) = 0 & \text{in } \Omega \\ \mathbf{u}(\mathbf{z}) = \mathbf{h}(\mathbf{z}) & \text{on } \partial\Omega_{\text{in}} \\ \mathbf{u}(\mathbf{z}) = \mathbf{0} & \text{on } \partial\Omega_{\text{lat}} \\ [(\nu\,\nabla\mathbf{u} - p\mathbb{I})\mathbf{n}](\mathbf{z}) = \mathbf{0} & \text{on } \partial\Omega_{\text{out}}, \end{cases} \tag{1}$$

completed with a prescribed velocity at the inlet section, $\partial\Omega_{\text{in}}$, no slip conditions on the wall boundary, $\partial\Omega_{\text{lat}}$, and do nothing boundary conditions on the outflow section, $\partial\Omega_{\text{out}}$, with $\partial\Omega_{\text{in}}$, $\partial\Omega_{\text{lat}}$, $\partial\Omega_{\text{out}}$ such that $\partial\Omega_{\text{in}} \cap \partial\Omega_{\text{lat}} \cap \partial\Omega_{\text{out}} = \emptyset$ and $\overline{\partial\Omega}_{\text{in}} \cup \overline{\partial\Omega}_{\text{lat}} \cup \overline{\partial\Omega}_{\text{out}} = \partial\Omega$. Here, ν is the kinematic viscosity, $\mathbf{u}(\mathbf{z}) = [u_1(\mathbf{z}), u_2(\mathbf{z})]^T$ is the velocity field, $p = p(\mathbf{z})$ denotes the pressure field, $\mathbf{f}(\mathbf{z}) = [f_1(\mathbf{z}), f_2(\mathbf{z})]^T$ is the force per unit mass, $\mathbf{h} = \mathbf{h}(\mathbf{z})$ is a given inflow profile, $\mathbb{I}$ is the identity tensor, $\mathbf{n} = \mathbf{n}(\mathbf{z})$ is the unit outward normal vector to the domain boundary, and $\mathbf{z} = (x_1, x_2)$ is the generic point in Ω. Without loss of generality, in the sequel, we assume $\mathbf{h}(\mathbf{z}) = \mathbf{0}$.

The weak formulation of problem (1) is: given $\nu \in \mathbb{R}^+$ and $\mathbf{f} \in L^2(\Omega;\mathbb{R}^2)$, find $\mathbf{u} \in V$ and $p \in Q$ such that

$$\begin{cases} a(\mathbf{u},\mathbf{v}) + b(\mathbf{v},p) = F(\mathbf{v}) & \forall \mathbf{v} \in V \\ b(\mathbf{u},q) = 0 & \forall q \in Q, \end{cases} \tag{2}$$

with $V = H^1_{\partial\Omega_{\text{in}}\cup\partial\Omega_{\text{lat}}}(\Omega;\mathbb{R}^2) = \left\{\mathbf{v} \in H^1(\Omega;\mathbb{R}^2) : \mathbf{v}(\mathbf{z}) = \mathbf{0} \text{ a.e. on } \partial\Omega_{\text{in}} \cup \partial\Omega_{\text{lat}}\right\}$ and $Q = L^2(\Omega)$, $a(\cdot,\cdot) : V \times V \to \mathbb{R}$, $b(\cdot,\cdot) : V \times Q \to \mathbb{R}$ and $F(\cdot) : V \to \mathbb{R}$ the bilinear and the linear forms defined by

$$a(\mathbf{u},\mathbf{v}) = \nu \int_\Omega \nabla\mathbf{u}(\mathbf{z}) : \nabla\mathbf{v}(\mathbf{z})\, d\mathbf{z}, \qquad b(\mathbf{v},p) = -\int_\Omega p(\mathbf{z})\, \nabla\cdot\mathbf{v}(\mathbf{z})\, d\mathbf{z},$$

$$F(\mathbf{v}) = \int_\Omega \mathbf{f}(\mathbf{z})\cdot\mathbf{v}(\mathbf{z})\, d\mathbf{z},$$

standard notation being adopted for the involved function spaces [27].
Problem (2) represents the so-called full problem to be discretized with the Hierarchical Model reduction. We observe that the regularity assumptions on the problem data guarantee the well-posedness of form (2) (see, e.g., [28, 27]).

2.1 HiMod reduction basics

Hierarchical Model (HiMod) reduction hinges on two main assumptions, namely the domain Ω exhibits a fiber bundle structure and trial and test functions are expanded through a separation of variables paradigm. In more detail, the computational domain is given by $\Omega = \bigcup_{x_1\in\Omega_{1D}} \{x_1\} \times \gamma_{x_1}$, where $\Omega_{1D} = (0, L) \subset \mathbb{R}$ is the leading fiber aligned with the mainstream, while $\{\gamma_{x_1}\}_{x_1\in\Omega_{1D}}$ denotes a set of transverse fibers parallel to the secondary dynamics. For computational convenience, the physical domain Ω is mapped into the reference domain

$\hat{\Omega} = \hat{\Omega}_{1D} \times \hat{\gamma}$, with $\hat{\Omega}_{1D} = \hat{\gamma} = (0,1)$, through the map $\boldsymbol{\Psi} : \Omega \to \hat{\Omega}$, such that $\boldsymbol{\Psi}(\mathbf{z}) = (\Psi_1(\mathbf{z}), \Psi_2(\mathbf{z})) = (\hat{x}_1, \hat{x}_2) = \hat{\mathbf{z}}$. The Jacobian associated with map $\boldsymbol{\Psi}$ is denoted by

$$J(\mathbf{z}) = \frac{\partial \boldsymbol{\Psi}(\mathbf{z})}{\partial \mathbf{z}} = \begin{pmatrix} \dfrac{\partial \Psi_1(\mathbf{z})}{\partial x_1} & \dfrac{\partial \Psi_1(\mathbf{z})}{\partial x_2} \\ \dfrac{\partial \Psi_2(\mathbf{z})}{\partial x_1} & \dfrac{\partial \Psi_2(\mathbf{z})}{\partial x_2} \end{pmatrix}. \tag{3}$$

We assume that map $\boldsymbol{\Psi}$ is invertible, with inverse $\boldsymbol{\Phi} : \hat{\Omega} \to \Omega$ such that $\boldsymbol{\Phi}(\hat{\mathbf{z}}) = (\Phi_1(\hat{\mathbf{z}}), \Phi_2(\hat{\mathbf{z}})) = (x_1, x_2) = \mathbf{z}$. Regularity assumptions are made on both $\boldsymbol{\Psi}$ and $\boldsymbol{\Phi}$, by requiring that $\boldsymbol{\Psi} \in C^1(\Omega; \mathbb{R}^2) \cap C^0(\overline{\Omega}; \mathbb{R}^2)$.
Maps $\boldsymbol{\Psi}$ and $\boldsymbol{\Phi}$ are used to relate corresponding boundary portions of Ω and $\hat{\Omega}$, so that we define $\partial\hat{\Omega}_{\mathrm{b}} = \boldsymbol{\Psi}(\partial\Omega_{\mathrm{b}})$, with $\mathrm{b} \in \{\mathrm{in}, \mathrm{lat}, \mathrm{out}\}$. We assume that the inflow (outflow) boundary of the physical domain is entirely mapped onto the left (right) side of the reference domain, namely, for any $\mathbf{z} \in \partial\Omega_{\mathrm{in}}$ ($\partial\Omega_{\mathrm{out}}$), $\Psi(\mathbf{z})$ is such that $\hat{x}_1 = 0$ ($\hat{x}_1 = 1$) while $\hat{x}_2 \in \hat{\gamma}$. As a result, the lateral walls of Ω are mapped onto the top and bottom sides of $\hat{\Omega}$. We remark that the regularity hypotheses on $\boldsymbol{\Psi}$ and $\boldsymbol{\Phi}$ allow to extend the map continuity up to $\partial\Omega$, allowing for sufficiently smooth boundary transformations.

In accordance with a separation of variables criterion, we introduce the function spaces

$$\hat{V}_{1D} = H^1_{\{0\}}(\hat{\Omega}_{1D}; \mathbb{R}^2) = \left\{ \hat{\mathbf{v}} \in H^1(\hat{\Omega}_{1D}; \mathbb{R}^2) : \hat{\mathbf{v}}(0) = \mathbf{0} \right\}, \qquad \hat{Q}_{1D} = L^2(\hat{\Omega}_{1D})$$

associated with $\hat{\Omega}_{1D}$ and the modal bases

$$B_v = \{T_i\}_{i=1}^m, \qquad B_q = \{R_j\}_{j=1}^n \tag{4}$$

defined on $\hat{\gamma}$, that we use to approximate the velocity and the pressure along the mainstream and the transverse direction, respectively with m, $n \in \mathbb{N}^*$ the modal indices. In particular, we add the following assumptions on the modal functions T_i and R_j:

$$T_i \in C^1(\overline{\hat{\gamma}}) \ \text{ and } \ \int_{\hat{\gamma}} T_i(\hat{x}_2)\, T_k(\hat{x}_2)\, d\hat{x}_2 = \delta_{ik} \qquad i,k = 1, \dots, m \tag{A1}$$

with δ_{ik} the Kronecker symbol;

$$R_j \in C^0(\overline{\hat{\gamma}}) \ \text{ and } \ \int_{\hat{\gamma}} R_j(\hat{x}_2)\, R_l(\hat{x}_2)\, d\hat{x}_2 = \delta_{jl} \qquad j,l = 1, \dots, n. \tag{A2}$$

The Dirichlet boundary conditions for $\mathbf{u}$ on $\partial\Omega_{\mathrm{in}}$ (i.e., on $\partial\hat{\Omega}_{\mathrm{in}}$) are enforced in the definition of $\hat{V}_{1D}$, whereas the boundary data on $\partial\Omega_{\mathrm{lat}}$ (i.e., on $\partial\hat{\Omega}_{\mathrm{lat}}$) are properly taken into account by the modal functions in B_v through the educated basis approach (see [11] for all the details). For instance, the assignment of a homogeneous Dirichlet condition on $\partial\Omega_{\mathrm{lat}}$ in (1) often leads to identifying modes T_i and R_j in (4) with standard trigonometric functions.

Thus, the HiMod function spaces to surrogate the velocity and the pressure

in (2) can be defined by

$$V_m = \left\{ \mathbf{v}_m(\mathbf{z}) = \mathbf{v}_m(x_1, x_2) = \sum_{i=1}^{m} \hat{\mathbf{v}}_i(\Psi_1(\mathbf{z}))T_i(\Psi_2(\mathbf{z})),\ \hat{\mathbf{v}}_i \in \hat{V}_{1D} \right\},$$
$$Q_n = \left\{ q_n(\mathbf{z}) = q_n(x_1, x_2) = \sum_{j=1}^{n} \hat{q}_j(\Psi_1(\mathbf{z}))R_j(\Psi_2(\mathbf{z})),\ \hat{q}_j \in \hat{Q}_{1D} \right\}, \tag{5}$$

respectively, where the HiMod coefficients $\{\hat{\mathbf{v}}_i\}_{i=1}^m$ and $\{\hat{q}_j\}_{j=1}^n$ are collected into the vectors $\hat{\mathbf{V}}_m \in \mathbb{V}_{m,x} := [\hat{V}_{1D}]^m$, $\hat{\mathbf{Q}}_n \in \mathbb{Q}_{n,x} := [\hat{Q}_{1D}]^n$, with

$$\hat{\mathbf{V}}_m = \hat{\mathbf{V}}_m(\hat{x}_1) = [\hat{\mathbf{v}}_1, \hat{\mathbf{v}}_2, \ldots, \hat{\mathbf{v}}_m]^T, \qquad \hat{\mathbf{Q}}_n = \hat{\mathbf{Q}}_n(\hat{x}_1) = [\hat{q}_1, \hat{q}_2, \ldots, \hat{q}_n]^T, \tag{6}$$

being $\hat{\mathbf{v}}_i = \hat{\mathbf{v}}_i(\hat{x}_1) = [\hat{v}_{i,1}(\hat{x}_1), \hat{v}_{i,2}(\hat{x}_1)]^T$ and $\hat{q}_j = \hat{q}_j(\hat{x}_1)$. Definitions (5) and (6) allow us to introduce a bijection between $\mathbb{V}_{m,x}$ and V_m as well as between $\mathbb{Q}_{n,x}$ and Q_n, since, for each vector $\hat{\mathbf{G}}_m = \hat{\mathbf{G}}_m(\hat{x}_1) = [\hat{\mathbf{g}}_1, \hat{\mathbf{g}}_2, \ldots, \hat{\mathbf{g}}_m]^T \in \mathbb{V}_{m,x}$ and $\hat{\mathbf{H}}_n = \hat{\mathbf{H}}_n(\hat{x}_1) = [\hat{h}_1, \hat{h}_2, \ldots, \hat{h}_n]^T \in \mathbb{Q}_{n,x}$, we can define the HiMod functions

$$\mathbf{g}_m(\mathbf{z}) = \mathbf{g}_m(x_1, x_2) = \sum_{i=1}^{m} \hat{\mathbf{g}}_i(\Psi_1(\mathbf{z}))T_i(\Psi_2(\mathbf{z})) \in V_m,$$
$$h_n(\mathbf{z}) = h_n(x_1, x_2) = \sum_{j=1}^{n} \hat{h}_j(\Psi_1(\mathbf{z}))R_j(\Psi_2(\mathbf{z})) \in Q_n,$$

and vice versa. Following the seminal work [9], we enforce a conformity condition on the HiMod spaces in (5), requiring that $V_m \subset V$ and $Q_n \subset Q$.
Spaces V_m and Q_n identify a hierarchy of reduced models according to the values of the modal indices m and n. In principle, we can employ a different number, m_1 and m_2, of modal basis functions for the two velocity components, although, for our purposes, we select $m_1 = m_2 = m$, following [11, 17]. The specific values of m and n can be chosen *a priori* (e.g., based on physical considerations) or determined automatically through an *a posteriori* modeling error analysis (see, e.g., [22, 23]). However, to ensure that the HiMod discretization preserves the stability properties of the full-order model (see, e.g., [28]), it is crucial to adjust indices m and n appropriately with respect to one another. This critical issue, which represents the key focus of the paper, will be thoroughly analyzed in the upcoming sections.

2.2 The HiMod formulation

The introduction of the reduced spaces in (5) allows us to provide the semi-discrete[1] HiMod formulation for the Stokes problem (2) in a straightforward way: for m, $n \in \mathbb{N}^*$, find $\mathbf{u}_m \in V_m$ and $p_n \in Q_n$ such that

$$\begin{cases} a(\mathbf{u}_m, \mathbf{w}) + b(\mathbf{w}, p_n) = F(\mathbf{w}) & \forall \mathbf{w} \in V_m \\ b(\mathbf{u}_m, z) = 0 & \forall z \in Q_n. \end{cases} \tag{7}$$

[1]The term semi-discrete refers to the fact that, at this stage, the leading direction remains continuous. This contrasts with the fully discrete HiMod formulation, where discretization is applied in both directions.

By exploiting the separation of variables characterizing the reduced spaces (5), it is well-known that a HiMod approximation leads to solve a system of coupled one-dimensional (1D) problems in $\hat{\Omega}_{1D}$, independently of the dimensionality of the full model [8, 9]. This reduced representation ensures a significant computational saving without compromising the accuracy of the HiMod solution (see, e.g., [17, 10, 18] for different application contexts).

In order to take advantage of a HiMod reduction for the Stokes problem as well, in (7) we exploit the HiMod expansion for the velocity and the pressure, i.e., we select

$$\mathbf{u}_m(\mathbf{z}) = \sum_{k=1}^{m} \hat{\mathbf{u}}_k(\Psi_1(\mathbf{z}))T_k(\Psi_2(\mathbf{z})), \qquad p_n(\mathbf{z}) = \sum_{j=1}^{n} \hat{p}_j(\Psi_1(\mathbf{z}))R_j(\Psi_2(\mathbf{z})), \quad (8)$$

and we choose the associated test functions as

$$\mathbf{w}_i(\mathbf{z}) = \hat{\mathbf{w}}_i(\Psi_1(\mathbf{z}))T_i(\Psi_2(\mathbf{z})), \qquad z_l(\mathbf{z}) = \hat{z}_l(\Psi_1(\mathbf{z}))R_l(\Psi_2(\mathbf{z})),$$

with $\hat{\mathbf{w}}_i = \hat{\mathbf{w}}_i(\hat{x}_1) = [\hat{w}_{i,1}(\hat{x}_1), \hat{w}_{i,2}(\hat{x}_1)]^T \in \hat{V}_{1D}$ and $\hat{z}_l \in \hat{Q}_{1D}$, for $i = 1, \dots, m$, and $l = 1, \dots, n$. We observe that modal coefficients $\{\hat{\mathbf{u}}_k\}_{k=1}^m$ and $\{\hat{p}_j\}_{j=1}^n$ are the unknowns of the HiMod formulation in (7).
Now, the bilinear forms involved in (7) can be written by leveraging the expression for the gradient and the divergence operators of a generic function $\mathbf{v}_m \in V_m$, given by

$$\left[\nabla \mathbf{v}_m(\mathbf{z})\right]_{st} = \sum_{i=1}^{m} \left[\hat{v}'_{i,s}(\Psi_1(\mathbf{z})) \frac{\partial \Psi_1(\mathbf{z})}{\partial x_t} T_i(\Psi_2(\mathbf{z})) + \hat{v}_{i,s}(\Psi_1(\mathbf{z})) T'_i(\Psi_2(\mathbf{z})) \frac{\partial \Psi_2(\mathbf{z})}{\partial x_t} \right],$$

with $s, t = 1, 2$, and

$$\nabla \cdot \mathbf{v}_m(\mathbf{z}) = \sum_{i=1}^{m} \sum_{s=1}^{2} \left[\hat{v}'_{i,s}(\Psi_1(\mathbf{z})) \frac{\partial \Psi_1(\mathbf{z})}{\partial x_s} T_i(\Psi_2(\mathbf{z})) + \hat{v}_{i,s}(\Psi_1(\mathbf{z})) T'_i(\Psi_2(\mathbf{z})) \frac{\partial \Psi_2(\mathbf{z})}{\partial x_s} \right],$$

respectively. In addition, we introduce the quantities

$$\mathcal{M}_1(\mathbf{\Phi}(\hat{\mathbf{z}})) = \sum_{t=1}^{2} \left(\frac{\partial \Psi_1(\mathbf{\Phi}(\hat{\mathbf{z}}))}{\partial x_t} \right)^2, \qquad \mathcal{M}_2(\mathbf{\Phi}(\hat{\mathbf{z}})) = \sum_{t=1}^{2} \left(\frac{\partial \Psi_2(\mathbf{\Phi}(\hat{\mathbf{z}}))}{\partial x_t} \right)^2,$$
$$\mathcal{M}_{12}(\mathbf{\Phi}(\hat{\mathbf{z}})) = \sum_{t=1}^{2} \left(\frac{\partial \Psi_1(\mathbf{\Phi}(\hat{\mathbf{z}}))}{\partial x_t} \frac{\partial \Psi_2(\mathbf{\Phi}(\hat{\mathbf{z}}))}{\partial x_t} \right), \quad (9)$$

associated with the components of the Jacobian in (3), together with the func-

tions

$$
\begin{aligned}
\mathcal{A}_{cd}^{0,0}(\hat{x}_1) &= \int_{\hat{\gamma}} T_c(\hat{x}_2) T_d(\hat{x}_2) \mathcal{M}_1(\mathbf{\Phi}(\hat{\mathbf{z}})) j(\hat{\mathbf{z}})\, d\hat{x}_2, \\
\mathcal{A}_{cd}^{1,0}(\hat{x}_1) = \mathcal{A}_{dc}^{0,1}(\hat{x}_1) &= \int_{\hat{\gamma}} T_c'(\hat{x}_2) T_d(\hat{x}_2) \mathcal{M}_{12}(\mathbf{\Phi}(\hat{\mathbf{z}})) j(\hat{\mathbf{z}})\, d\hat{x}_2, \\
\mathcal{A}_{cd}^{0,1}(\hat{x}_1) = \mathcal{A}_{dc}^{1,0}(\hat{x}_1) &= \int_{\hat{\gamma}} T_c(\hat{x}_2) T_d'(\hat{x}_2) \mathcal{M}_{12}(\mathbf{\Phi}(\hat{\mathbf{z}})) j(\hat{\mathbf{z}})\, d\hat{x}_2, \\
\mathcal{A}_{cd}^{1,1}(\hat{x}_1) &= \int_{\hat{\gamma}} T_c'(\hat{x}_2) T_d'(\hat{x}_2) \mathcal{M}_2(\mathbf{\Phi}(\hat{\mathbf{z}})) j(\hat{\mathbf{z}})\, d\hat{x}_2, \\
\mathcal{B}_{df,s}^{0,0}(\hat{x}_1) &= \int_{\hat{\gamma}} T_d(\hat{x}_2) R_f(\hat{x}_2) J_{1s}(\mathbf{\Phi}(\hat{\mathbf{z}})) j(\hat{\mathbf{z}})\, d\hat{x}_2, \\
\mathcal{B}_{df,s}^{1,0}(\hat{x}_1) &= \int_{\hat{\gamma}} T_d'(\hat{x}_2) R_f(\hat{x}_2) J_{2s}(\mathbf{\Phi}(\hat{\mathbf{z}})) j(\hat{\mathbf{z}})\, d\hat{x}_2,
\end{aligned}
\tag{10}
$$

which compress the information associated with the bilinear forms $a(\cdot,\cdot)$, $b(\cdot,\cdot)$ along the transverse fiber $\hat{\gamma}$, respectively for $c,\ d = 1,\dots,m,\ f = 1,\dots,n$, with J_{gh} the components of the Jacobian matrix in (3) for $g,\ h = 1,2$, and $j(\hat{\mathbf{z}}) = \left|\det(J^{-1}(\Phi(\hat{\mathbf{z}})))\right|$.

Thus, by exploiting the definitions in (9) and (10) and the separation of variables intrinsic to the HiMod reduction, we can expand the viscous contribution in (7) as

$$
\begin{aligned}
a(\mathbf{u}_m, \mathbf{w}_i) &= \nu \sum_{k=1}^{m} \int_{\hat{\Omega}} \Bigg\{ \Bigg(\sum_{s=1}^{2} \hat{u}_{k,s}'(\hat{x}_1) \hat{w}_{i,s}'(\hat{x}_1) \Bigg) T_k(\hat{x}_2) T_i(\hat{x}_2) \mathcal{M}_1(\mathbf{\Phi}(\hat{\mathbf{z}})) \\
&+ \Bigg(\sum_{s=1}^{2} \hat{u}_{k,s}'(\hat{x}_1) \hat{w}_{i,s}(\hat{x}_1) \Bigg) T_k(\hat{x}_2) T_i'(\hat{x}_2) \mathcal{M}_{12}(\mathbf{\Phi}(\hat{\mathbf{z}})) \\
&+ \Bigg(\sum_{s=1}^{2} \hat{u}_{k,s}(\hat{x}_1) \hat{w}_{i,s}'(\hat{x}_1) \Bigg) T_k'(\hat{x}_2) T_i(\hat{x}_2) \mathcal{M}_{12}(\mathbf{\Phi}(\hat{\mathbf{z}})) \\
&+ \Bigg(\sum_{s=1}^{2} \hat{u}_{k,s}(\hat{x}_1) \hat{w}_{i,s}(\hat{x}_1) \Bigg) T_k'(\hat{x}_2) T_i'(\hat{x}_2) \mathcal{M}_2(\mathbf{\Phi}(\hat{\mathbf{z}})) \Bigg\}\, d\hat{\mathbf{z}} \\
&= \nu \sum_{k=1}^{m} \int_{\hat{\Omega}_{1D}} \Bigg\{ \Bigg(\sum_{s=1}^{2} \hat{u}_{k,s}'(\hat{x}_1) \hat{w}_{i,s}'(\hat{x}_1) \Bigg) \mathcal{A}_{ki}^{0,0}(\hat{x}_1) \\
&+ \Bigg(\sum_{s=1}^{2} \hat{u}_{k,s}'(\hat{x}_1) \hat{w}_{i,s}(\hat{x}_1) \Bigg) \mathcal{A}_{ki}^{0,1}(\hat{x}_1) \\
&+ \Bigg(\sum_{s=1}^{2} \hat{u}_{k,s}(\hat{x}_1) \hat{w}_{i,s}'(\hat{x}_1) \Bigg) \mathcal{A}_{ki}^{1,0}(\hat{x}_1) \\
&+ \Bigg(\sum_{s=1}^{2} \hat{u}_{k,s}(\hat{x}_1) \hat{w}_{i,s}(\hat{x}_1) \Bigg) \mathcal{A}_{ki}^{1,1}(\hat{x}_1) \Bigg\}\, d\hat{x}_1
\end{aligned}
\tag{11}
$$

for $i = 1, \dots, m$, while the terms associated with the divergence operator are equivalent to

$$
\begin{aligned}
b(\mathbf{w}_i, p_n) = &- \sum_{j=1}^{n} \int_{\hat{\Omega}} \Bigg\{ \sum_{s=1}^{2} \Big[\hat{w}'_{i,s}(\hat{x}_1) \hat{p}_j(\hat{x}_1) T_i(\hat{x}_2) R_j(\hat{x}_2) J_{1s}(\mathbf{\Phi}(\hat{\mathbf{z}})) \\
&+ \hat{w}_{i,s}(\hat{x}_1) \hat{p}_j(\hat{x}_1) T'_i(\hat{x}_2) R_j(\hat{x}_2) J_{2s}(\mathbf{\Phi}(\hat{\mathbf{z}})) \Big] \Bigg\} j(\hat{\mathbf{z}})\, d\hat{\mathbf{z}} \\
= &- \sum_{j=1}^{n} \int_{\hat{\Omega}_{1D}} \sum_{s=1}^{2} \Big[\hat{w}'_{i,s}(\hat{x}_1) \hat{p}_j(\hat{x}_1) \mathcal{B}^{0,0}_{ij,s}(\hat{x}_1) + \hat{w}_{i,s}(\hat{x}_1) \hat{p}_j(\hat{x}_1) \mathcal{B}^{1,0}_{ij,s}(\hat{x}_1) \Big] \, d\hat{x}_1
\end{aligned}
\tag{12}
$$

for $i = 1, \dots, m$ and

$$
\begin{aligned}
b(\mathbf{u}_m, z_l) = &- \sum_{k=1}^{m} \int_{\hat{\Omega}} \Bigg\{ \sum_{s=1}^{2} \Big[\hat{u}'_{k,s}(\hat{x}_1) \hat{z}_l(\hat{x}_1) T_k(\hat{x}_2) R_l(\hat{x}_2) J_{1s}(\mathbf{\Phi}(\hat{\mathbf{z}})) \\
&+ \hat{u}_{k,s}(\hat{x}_1) \hat{z}_l(\hat{x}_1) T'_k(\hat{x}_2) R_l(\hat{x}_2) J_{2s}(\mathbf{\Phi}(\hat{\mathbf{z}})) \Big] \Bigg\} j(\hat{\mathbf{z}})\, d\hat{\mathbf{z}} \\
= &- \sum_{k=1}^{m} \int_{\hat{\Omega}_{1D}} \sum_{s=1}^{2} \Big[\hat{u}'_{k,s}(\hat{x}_1) \hat{z}_l(\hat{x}_1) \mathcal{B}^{0,0}_{kl,s}(\hat{x}_1) + \hat{u}_{k,s}(\hat{x}_1) \hat{z}_l(\hat{x}_1) \mathcal{B}^{1,0}_{kl,s}(\hat{x}_1) \Big] \, d\hat{x}_1,
\end{aligned}
\tag{13}
$$

for $l = 1, \dots, n$, respectively. Finally, the forcing term in (7) is commuted into

$$
\begin{aligned}
F(\mathbf{w}_i) &= \int_{\hat{\Omega}} \Big[f_1(\mathbf{\Phi}(\hat{\mathbf{z}})) \hat{w}_{i,1}(\hat{x}_1) T_i(\hat{x}_2) + f_2(\mathbf{\Phi}(\hat{\mathbf{z}})) \hat{w}_{i,2}(\hat{x}_1) T_i(\hat{x}_2) \Big] j(\hat{\mathbf{z}})\, d\hat{\mathbf{z}} \\
&= \int_{\hat{\Omega}_{1D}} \sum_{s=1}^{2} \Big[\hat{w}_{i,s}(\hat{x}_1) \int_{\hat{\gamma}} T_i(\hat{x}_2) f_s(\mathbf{\Phi}(\hat{\mathbf{z}})) j(\hat{\mathbf{z}})\, d\hat{x}_2 \Big] \, d\hat{x}_1.
\end{aligned}
\tag{14}
$$

for $i = 1, \dots, m$. The expansions in (11)–(14) can alternatively be expressed in a more compact form, by introducing suitable arrays, consistent with the definitions in (6). Indeed, we consider: vectors

$$
\hat{\mathbf{U}}_m = \hat{\mathbf{U}}_m(\hat{x}_1) = [\hat{\mathbf{u}}_1, \hat{\mathbf{u}}_2, \dots, \hat{\mathbf{u}}_m]^T \in \mathbb{V}_{m,x},
$$

$$
\hat{\mathbf{P}}_n = \hat{\mathbf{P}}_n(\hat{x}_1) = [\hat{p}_1, \hat{p}_2, \dots, \hat{p}_n]^T \in \mathbb{Q}_{n,x},
$$

gathering the (unknown) modal coefficients for the HiMod velocity and pressure in (8), with $\hat{\mathbf{u}}_k = \hat{\mathbf{u}}_k(\hat{x}_1) = [\hat{u}_{k,1}(\hat{x}_1), \hat{u}_{k,2}(\hat{x}_1)]^T$ for $k = 1, \dots, m$, and $\hat{p}_j = \hat{p}_j(\hat{x}_1)$ for $j = 1, \dots, n$, together with vectors

$$
\hat{\mathbf{W}}_m = \hat{\mathbf{W}}_m(\hat{x}_1) = [\hat{\mathbf{w}}_1, \hat{\mathbf{w}}_2, \dots, \hat{\mathbf{w}}_m]^T \in \mathbb{V}_{m,x},
$$

$$
\hat{\mathbf{Z}}_n = \hat{\mathbf{Z}}_n(\hat{x}_1) = [\hat{z}_1, \hat{z}_2, \dots, \hat{z}_n]^T \in \mathbb{Q}_{n,x},
$$

associated with the test functions for the momentum and continuity equation, respectively with $\hat{\mathbf{w}}_i = \hat{\mathbf{w}}_i(\hat{x}_1) = [\hat{w}_{i,1}(\hat{x}_1), \hat{w}_{i,2}(\hat{x}_1)]^T$ for $i = 1, \dots, m$, and $\hat{z}_l = \hat{z}_l(\hat{x}_1)$ for $l = 1, \dots, n$; the $2m \times 2m$ block matrices of functions $\mathbf{A}^{0,0} = \mathbf{A}^{0,0}(\hat{x}_1)$, $\mathbf{A}^{0,1} = \mathbf{A}^{0,1}(\hat{x}_1)$, $\mathbf{A}^{1,0} = \mathbf{A}^{1,0}(\hat{x}_1)$, $\mathbf{A}^{1,1} = \mathbf{A}^{1,1}(\hat{x}_1)$. In particular,

matrix $\mathbf{A}^{q,r}$ consists of $m \times m$ blocks of order 2, such that the block in position ik, $\left[\mathbf{A}^{q,r}\right]_{B_{ik}} = \left[\mathbf{A}^{q,r}(\hat{x}_1)\right]_{B_{ik}}$, is given by

$$\left[\mathbf{A}^{q,r}\right]_{B_{ik}} = \mathrm{diag}(\mathcal{A}_{ik}^{q,r}, \mathcal{A}_{ik}^{q,r})$$

for $i, k = 1, \ldots, m$, and $q, r = 0, 1$; the $2m \times n$ block matrices of functions $\mathbf{B}^{0,0} = \mathbf{B}^{0,0}(\hat{x}_1)$, $\mathbf{B}^{1,0} = \mathbf{B}^{1,0}(\hat{x}_1)$ which collect, by rows, the m blocks

$$\left[\mathbf{B}^{q,0}\right]_{B_i} = \begin{bmatrix} \mathcal{B}_{i1,1}^{q,0} & \mathcal{B}_{i2,1}^{q,0} & \ldots & \ldots \mathcal{B}_{in,1}^{q,0} \\ \mathcal{B}_{i1,2}^{q,0} & \mathcal{B}_{i2,2}^{q,0} & \ldots & \ldots \mathcal{B}_{in,2}^{q,0} \end{bmatrix} \in \mathbb{R}^{2\times n} \tag{15}$$

for $i = 1, \ldots, m$ and $q = 0, 1$. Thus, the HiMod formulation (7) can be equivalently reformulated as: for m, $n \in \mathbb{N}^*$, find $\hat{\mathbf{U}}_m \in \mathbb{V}_{m,x}$ and $\hat{\mathbf{P}}_n \in \mathbb{Q}_{n,x}$ such that

$$\begin{cases} \tilde{a}(\hat{\mathbf{U}}_m, \hat{\mathbf{W}}_m) + \tilde{b}(\hat{\mathbf{W}}_m, \hat{\mathbf{P}}_n) = \tilde{F}(\hat{\mathbf{W}}_m) & \forall \hat{\mathbf{W}}_m \in \mathbb{V}_{m,x} \\ \tilde{b}(\hat{\mathbf{U}}_m, \hat{\mathbf{Z}}_n) = 0 & \forall \hat{\mathbf{Z}}_n \in \mathbb{Q}_{n,x}, \end{cases} \tag{16}$$

where

$$\begin{aligned} \tilde{a}(\hat{\mathbf{U}}_m, \hat{\mathbf{W}}_m) &= \nu \int_{\hat{\Omega}_{1D}} \Big\{ \left[\hat{\mathbf{W}}'_m\right]^T \mathbf{A}^{0,0}\, \hat{\mathbf{U}}'_m + \left[\hat{\mathbf{W}}_m\right]^T \mathbf{A}^{1,0}\, \hat{\mathbf{U}}'_m \\ &\qquad + \left[\hat{\mathbf{W}}'_m\right]^T \mathbf{A}^{0,1}\, \hat{\mathbf{U}}_m + \left[\hat{\mathbf{W}}_m\right]^T \mathbf{A}^{1,1}\, \hat{\mathbf{U}}_m \Big\}\, d\hat{x}_1 \\ \tilde{b}(\hat{\mathbf{W}}_m, \hat{\mathbf{P}}_n) &= -\int_{\hat{\Omega}_{1D}} \Big\{ \left[\hat{\mathbf{W}}'_m\right]^T \mathbf{B}^{0,0}\, \hat{\mathbf{P}}_n + \left[\hat{\mathbf{W}}_m\right]^T \mathbf{B}^{1,0}\, \hat{\mathbf{P}}_n \Big\}\, d\hat{x}_1 \\ \tilde{b}(\hat{\mathbf{U}}_m, \hat{\mathbf{Z}}_n) &= -\int_{\hat{\Omega}_{1D}} \Big\{ \left[\hat{\mathbf{Z}}_n\right]^T [\mathbf{B}^{0,0}]^T\, \hat{\mathbf{U}}'_m + \left[\hat{\mathbf{Z}}_n\right]^T [\mathbf{B}^{1,0}]^T\, \hat{\mathbf{U}}_m \Big\}\, d\hat{x}_1 \\ \tilde{F}(\hat{\mathbf{W}}_m) &= \int_{\hat{\Omega}_{1D}} [\hat{\mathbf{W}}_m]^T\, \hat{\mathbf{F}}_m\, d\hat{x}_1 \end{aligned} \tag{17}$$

where $\hat{\mathbf{F}}_m = \hat{\mathbf{F}}_m(\hat{x}_1)$ denotes the function vector with components

$$[\hat{\mathbf{F}}_m(\hat{x}_1)]_e = \begin{cases} \displaystyle\int_{\hat{\gamma}} T_i(\hat{x}_2) f_1(\mathbf{\Phi}(\hat{\mathbf{z}})) j(\hat{\mathbf{z}})\, d\hat{x}_2 & \text{if } e = 2i-1 \\ \displaystyle\int_{\hat{\gamma}} T_i(\hat{x}_2) f_2(\mathbf{\Phi}(\hat{\mathbf{z}})) j(\hat{\mathbf{z}})\, d\hat{x}_2 & \text{if } e = 2i \end{cases}$$

with $e = 1, \ldots, 2m$, for $i = 1, \ldots, m$. Problem (16) constitutes the reference formulation to carry out the well-posedness analysis in Sec. 4.

3 Preliminaries

This section lays the groundwork for establishing the well-posedness of (7), by collecting partial results needed to analyze the bilinear forms $\tilde{a}(\cdot,\cdot)$ and $\tilde{b}(\cdot,\cdot)$.

To this end, we denote by j_0 and j_1 the two strictly positive constants such that

$$0 < j_0 \le j(\hat{\mathbf{z}}) \le j_1 < +\infty \qquad \forall \hat{\mathbf{z}} \in \hat{\Omega}, \tag{18}$$

whose existence is guaranteed by the regularity assumptions made on the map $\mathbf{\Psi}$. In practice, the boundedness of j_1 ensures that an element of infinitesimal area, ε, in $\hat{\Omega}$ is transformed into an element in Ω with area bounded above by $j_1\varepsilon$, while inequality $j_0 > 0$ guarantees that two distinct points in $\hat{\Omega}$ cannot collapse into the same point in Ω.

In addition, we can properly bound some of the quantities strictly related to the map $\mathbf{\Psi}$, specifically $\mathcal{M}_1$, $\mathcal{M}_2$, $\mathcal{M}_{12}$ in (9), when multiplied by j. In particular, we have

$$\begin{gathered}\vartheta_0 \le \mathcal{M}_1(\mathbf{\Phi}(\hat{\mathbf{z}}))j(\hat{\mathbf{z}}) \le \vartheta_1, \qquad \xi_0 \le \mathcal{M}_2(\mathbf{\Phi}(\hat{\mathbf{z}}))j(\hat{\mathbf{z}}) \le \xi_1 \qquad \forall \hat{\mathbf{z}} \in \hat{\Omega}, \\ \left|\mathcal{M}_{12}(\mathbf{\Phi}(\hat{\mathbf{z}}))j(\hat{\mathbf{z}})\right| \le \pi_1 \qquad \forall \hat{\mathbf{z}} \in \hat{\Omega},\end{gathered} \tag{19}$$

for $0 < \vartheta_0 \le \vartheta_1 < +\infty$, $0 < \xi_0 \le \xi_1 < +\infty$ and $0 \le \pi_1 < +\infty$. In particular, it is the invertibility of the Jacobian in (3) that guarantees the strict positivity of the two lower bounds ϑ_0 and ξ_0.

With similar arguments, we can bound the Jacobian components J_{1s} and J_{2s} involved in (10), when multiplied by j, as

$$\left|J_{1s}(\mathbf{\Phi}(\hat{\mathbf{z}}))j(\hat{\mathbf{z}})\right| \le \gamma_s, \qquad \left|J_{2s}(\mathbf{\Phi}(\hat{\mathbf{z}}))j(\hat{\mathbf{z}})\right| \le \sigma_s \qquad \forall \hat{\mathbf{z}} \in \hat{\Omega} \tag{20}$$

for certain positive constants γ_s and σ_s and $s = 1, 2$.

We also introduce the $2m \times 2m$ block matrix of functions $\mathbf{A}^{1,1}_{\hat{\gamma}}$ consisting of $m \times m$ blocks of order 2, whose block in position ki is given by

$$\left[\mathbf{A}^{1,1}_{\hat{\gamma}}\right]_{B_{ki}} = \operatorname{diag}(\mathcal{A}^{1,1}_{\hat{\gamma},ki}, \mathcal{A}^{1,1}_{\hat{\gamma},ki}) \tag{21}$$

with

$$\mathcal{A}^{1,1}_{\hat{\gamma},ki} = \int_{\hat{\gamma}} T'_k(\hat{x}_2) T'_i(\hat{x}_2)\, d\hat{x}_2.$$

Notice that, for $k, i = 1, \ldots, m$, quantity $\mathcal{A}^{1,1}_{\hat{\gamma},ki}$ pushes back the stiffness matrix in $(10)_4$ to the reference fiber $\hat{\gamma}$. Matrix $\mathbf{A}^{1,1}_{\hat{\gamma}}$ is assumed to satisfy the two-sided inequality

$$\bar{\xi}_0 \le \lambda_{\min}(\mathbf{A}^{1,1}_{\hat{\gamma}}) \le \lambda_{\max}(\mathbf{A}^{1,1}_{\hat{\gamma}}) \le \bar{\xi}_1\, m^2 \tag{A3}$$

for certain positive constants $\bar{\xi}_0$, $\bar{\xi}_1$, with $\lambda_{\min}(\mathbf{A}^{1,1}_{\hat{\gamma}})$ and $\lambda_{\max}(\mathbf{A}^{1,1}_{\hat{\gamma}})$ the minimum and the maximum eigenvalue of the matrix $\mathbf{A}^{1,1}_{\hat{\gamma}}$.

Moreover, to prove the inf-sup property for the bilinear form $\tilde{b}(\cdot,\cdot)$, we will resort to a condensed counterpart, $\mathbf{B}^{0,0}_c = \mathbf{B}^{0,0}_c(\hat{x}_1)$, of matrix $B^{0,0}$ in (15), coinciding with a $n \times n$ array of functions whose i-th row is defined by

$$\left[\mathbf{B}^{0,0}_c\right]_i = \left[\mathcal{B}^{0,0}_{i1,1}, \mathcal{B}^{0,0}_{i2,1}, \ldots, \mathcal{B}^{0,0}_{in,1}\right] \in \mathbb{R}^n, \tag{22}$$

for $i = 1, \ldots, n$. Matrix $\mathbf{B}^{0,0}_c$ is assumed to satisfy the lower bound

$$\lambda_{\min}\left(\left[\mathbf{B}^{0,0}_c\right]^T \mathbf{B}^{0,0}_c\right) \ge \gamma_0^2\, n^{-1/4} \qquad \forall \hat{x}_1 \in \hat{\Omega}_{1D}, \tag{A4}$$

with $\gamma_0 > 0$.

Finally, we will exploit the spaces associated with $\hat{\gamma}$ spanned by the velocity and the pressure modal basis functions, i.e.,

$$\mathbb{V}_{m,y} = \text{span}\{T_i\}_{i=1}^{m}, \qquad \mathbb{Q}_{n,y} = \text{span}\{R_j\}_{j=1}^{n},$$

respectively. This allows us to establish a bijection between $\mathbb{R}^{2m}$ and $[\mathbb{V}_{m,y}]^2$ as well as between $\mathbb{R}^n$ and $\mathbb{Q}_{n,y}$. Indeed, for each vector $\mathbf{t} = [\mathbf{t}_1, \mathbf{t}_2, \dots, \mathbf{t}_m]^T \in \mathbb{R}^{2m}$, with $\mathbf{t}_i = [t_{i,1}, t_{i,2}]^T$ for $i = 1, \dots, m$, and $\mathbf{r} = [r_1, r_2, \dots, r_n]^T \in \mathbb{R}^n$, we can define the modal functions

$$\boldsymbol{\tau}_m(\hat{x}_2) = \sum_{i=1}^{m} \mathbf{t}_i T_i(\hat{x}_2) \in [\mathbb{V}_{m,y}]^2, \qquad \rho_n(\hat{x}_2) = \sum_{j=1}^{n} r_j R_j(\hat{x}_2) \in \mathbb{Q}_{n,y}, \tag{23}$$

and vice versa, with, thanks to assumptions (A1) and (A2),

$$\|\boldsymbol{\tau}_m\|_{L^2(\hat{\gamma})} = \|\mathbf{t}\|, \qquad \|\rho_n\|_{L^2(\hat{\gamma})} = \|\mathbf{r}\|, \tag{24}$$

respectively, $\|\cdot\|$ denoting the standard Euclidean norm.

The remaining part of the section is devoted to establishing auxiliary results relevant to the well-posedness analysis of formulation (7).

Lemma 1. *Under assumptions (A1) and (A3), we can prove the Poincaré-type inequality*

$$\|\boldsymbol{\tau}_m\|_{L^2(\hat{\gamma})} \leq (\bar{\xi}_0)^{-\frac{1}{2}} \|\boldsymbol{\tau}'_m\|_{L^2(\hat{\gamma})} \tag{25}$$

and the inverse-type inequality

$$\|\boldsymbol{\tau}'_m\|_{L^2(\hat{\gamma})} \leq (\bar{\xi}_1)^{\frac{1}{2}}\, m\, \|\boldsymbol{\tau}_m\|_{L^2(\hat{\gamma})}, \tag{26}$$

for any function $\boldsymbol{\tau}_m \in [\mathbb{V}_{m,y}]^2$, and with $\bar{\xi}_0$ and $\bar{\xi}_1$ defined as in (A3).

Proof. The bijection between $\mathbb{R}^{2m}$ and $[\mathbb{V}_{m,y}]^2$ in (23) when combined with the definition of $\mathbf{A}_{\hat{\gamma}}^{1,1}$ according to (21) justifies the equality

$$\|\boldsymbol{\tau}'_m\|^2_{L^2(\hat{\gamma})} = \mathbf{t}^T \mathbf{A}_{\hat{\gamma}}^{1,1} \mathbf{t}.$$

By exploiting the Rayleigh quotient definition and assumption (A3), we have

$$\bar{\xi}_0 \|\mathbf{t}\|^2 \leq \lambda_{\min}(\mathbf{A}_{\hat{\gamma}}^{1,1})\, \mathbf{t}^T\mathbf{t} \leq \|\boldsymbol{\tau}'_m\|^2_{L^2(\hat{\gamma})} = \mathbf{t}^T \mathbf{A}_{\hat{\gamma}}^{1,1} \mathbf{t} \leq \lambda_{\max}(\mathbf{A}_{\hat{\gamma}}^{1,1}) \mathbf{t}^T\mathbf{t} \leq \bar{\xi}_1 m^2 \|\mathbf{t}\|^2.$$

Now, thanks to assumption (A1), we use relation in $(24)_1$ to replace $\|\mathbf{t}\|$ with $\|\boldsymbol{\tau}_m\|_{L^2(\hat{\gamma})}$. This concludes the proof. □

Remark 3.1. *The deterioration of the upper bound in (26) as m increases is coherent with the spectral theory (see, e.g., [29]). This justifies the discrepancy (i.e., the dependence on m) between the lower and upper bounds in (A3).*

As a straightforward consequence of the above Lemma, we can state the following

Corollary 2. *Under assumptions (A1) and (A3), it can be proved that the derivatives of the modal functions T_i in B_v satisfy the following inequality*

$$\sum_{i=1}^{m} \|T'_i(\hat{x}_2)\|^2_{L^2(\hat{\gamma})} \leq \bar{\xi}_1\, m^3 \tag{27}$$

with $\bar{\xi}_1$ defined as in (A3).

Proof. We exploit the modal definition for $\boldsymbol{\tau}_m$ in $(23)_1$ to verify that

$$\|\boldsymbol{\tau}_m'\|^2_{L^2(\hat{\gamma})} = \int_{\hat{\gamma}} \left[T_i'(\hat{x}_2)\right]^2 d\hat{x}_2 = \|T_i'(\hat{x}_2)\|^2_{L^2(\hat{\gamma})}$$

when vector $\mathbf{t}$ in $(23)_1$ is chosen such that

$$[\mathbf{t}_j] = \begin{cases} [1\ 0]^T & \text{if } j = i \\ \mathbf{0} & \text{overwhise,} \end{cases}$$

with $\mathbf{0} \in \mathbb{R}^2$ the null vector. The norm equality in $(24)_1$, in combination with the inverse-type inequality in (26), guarantees that

$$\|\boldsymbol{\tau}_m'\|^2_{L^2(\hat{\gamma})} = \|T_i'(\hat{x}_2)\|^2_{L^2(\hat{\gamma})} \leq \bar{\xi}_1\, m^2\, \|\mathbf{t}\|^2 = \xi_1\, m^2$$

since $\|\mathbf{t}\|^2 = 1$. By summing over i, we have the desired result. □

The coercivity and the continuity properties of the bilinear form $\tilde{a}(\cdot,\cdot)$ will involve the result below.

Lemma 3. *Under assumptions (A1) and (A3), we can prove that*

1. *block matrices of functions $\mathbf{A}^{0,0}$ and $\mathbf{A}^{1,1}$ are symmetric positive definite for any $\hat{x}_1 \in \hat{\Omega}_{1D}$, and the following two-sided inequalities hold:*

$$\begin{aligned} \vartheta_0 \leq \lambda_{\min}(\mathbf{A}^{0,0}) \leq \lambda_{\max}(\mathbf{A}^{0,0}) \leq \vartheta_1 \qquad & \forall \hat{x}_1 \in \hat{\Omega}_{1D}, \\ \xi_0\ \bar{\xi}_0 \leq \lambda_{\min}(\mathbf{A}^{1,1}) \leq \lambda_{\max}(\mathbf{A}^{1,1}) \leq \xi_1\ \bar{\xi}_1\ m^2 \qquad & \forall \hat{x}_1 \in \hat{\Omega}_{1D}, \end{aligned} \tag{28}$$

   with ϑ_0, ϑ_1, ξ_0, ξ_1 are defined as in (19), while $\bar{\xi}_0$, $\bar{\xi}_1$ are the same as in (A3);

2. *the spectral norm of the block matrices of functions $\mathbf{A}^{1,0}$ and $\mathbf{A}^{0,1}$ can be bounded from above as*

$$\|\mathbf{A}^{1,0}\|_2^2 = \lambda_{\max}\big([\mathbf{A}^{1,0}]^T\mathbf{A}^{1,0}\big) \leq \pi_1^2\, \bar{\xi}_1\, m^3 \qquad \forall \hat{x}_1 \in \hat{\Omega}_{1D}, \tag{29}$$

$$\|\mathbf{A}^{0,1}\|_2^2 = \lambda_{\max}\big([\mathbf{A}^{0,1}]^T\mathbf{A}^{0,1}\big) \leq \pi_1^2\, \bar{\xi}_1\, m^3 \qquad \forall \hat{x}_1 \in \hat{\Omega}_{1D}, \tag{30}$$

   with π_1 defined as in $(19)_3$.

Proof. We start by considering the two-sided inequality in $(28)_1$. We take an arbitrary vector $\mathbf{t} \in \mathbb{R}^{2m}$ together with the associated function $\boldsymbol{\tau}_m$ according to $(23)_1$. Then, thanks to (A1), it holds

$$\begin{aligned} \mathbf{t}^T\mathbf{A}^{0,0}\mathbf{t} &= \sum_{i=1}^{m}\sum_{k=1}^{m} \int_{\hat{\gamma}} \mathbf{t}_k^T\mathbf{t}_i T_k(\hat{x}_2) T_i(\hat{x}_2) \mathcal{M}_1(\boldsymbol{\Phi}(\hat{\mathbf{z}})) j(\hat{\mathbf{z}})\, d\hat{x}_2 \\ &= \int_{\hat{\gamma}} [\boldsymbol{\tau}_m(\hat{x}_2)]^2 \mathcal{M}_1(\boldsymbol{\Phi}(\hat{\mathbf{z}})) j(\hat{\mathbf{z}})\, d\hat{x}_2. \end{aligned}$$

Now, thanks to the boundedness of $\mathcal{M}_1(\boldsymbol{\Phi}(\hat{\mathbf{z}}))j(\hat{\mathbf{z}})$ in $(19)_1$, we have

$$\vartheta_0 \|\boldsymbol{\tau}_m\|^2_{L^2(\hat{\gamma})} \leq \mathbf{t}^T\mathbf{A}^{0,0}\mathbf{t} \leq \vartheta_1 \|\boldsymbol{\tau}_m\|^2_{L^2(\hat{\gamma})}.$$

This leads to the inequality in $(28)_1$ after using the Rayleigh quotient definition and the norm equivalence in $(24)_1$ which is guaranteed by assumption (A1).
As far as $(28)_2$ is concerned, in a similar way we obtain

$$\xi_0 \|\boldsymbol{\tau}'_m\|^2_{L^2(\hat{\gamma})} \leq \mathbf{t}^T \mathbf{A}^{1,1} \mathbf{t} \leq \xi_1 \|\boldsymbol{\tau}'_m\|^2_{L^2(\hat{\gamma})}.$$

By applying the Poincaré inequality (25) and the inverse inequality (26) on the left- and on the right-hand side, respectively, combined with the Rayleigh quotient definition, we immediately obtain the desired control on the eigenvalues of $\mathbf{A}^{1,1}$ in $(28)_2$.
To prove result in (29), we first introduce vector $\mathbf{y} = \mathbf{A}^{1,0}\mathbf{t}$, where $\mathbf{y} = [\mathbf{y}_1, \mathbf{y}_2, \ldots, \mathbf{y}_m]^T$ with $\mathbf{y}_i = [y_{i,1}, y_{i,2}]^T$ for $i = 1, \ldots, m$, to write

$$\mathbf{y}_i = \sum_{k=1}^{m} \int_{\hat{\gamma}} \mathbf{t}_k T_k(\hat{x}_2)\ T'_i(\hat{x}_2)\ \mathcal{M}_{12}(\boldsymbol{\Phi}(\hat{\mathbf{z}}))j(\hat{\mathbf{z}})\, d\hat{x}_2.$$

As a consequence, using the explicit definition of matrix $\mathbf{A}^{1,0}$ as a block matrix with diagonal blocks, it turns out that

$$\begin{aligned}
\mathbf{y}^T\mathbf{y} &= \sum_{i=1}^{m} \left[\sum_{k=1}^{m} \int_{\hat{\gamma}} \mathbf{t}_k T_k(\hat{x}_2)\ T'_i(\hat{x}_2)\ \mathcal{M}_{12}(\boldsymbol{\Phi}(\hat{\mathbf{z}}))j(\hat{\mathbf{z}})\, d\hat{x}_2 \right]^2 \\
&= \sum_{i=1}^{m} \left[\int_{\hat{\gamma}} \boldsymbol{\tau}_m(\hat{x}_2)\ T'_i(\hat{x}_2)\ \mathcal{M}_{12}(\boldsymbol{\Phi}(\hat{\mathbf{z}}))j(\hat{\mathbf{z}})\, d\hat{x}_2 \right]^2 \\
&\leq \pi_1^2 \|\boldsymbol{\tau}_m\|^2_{L^2(\hat{\gamma})} \sum_{i=1}^{m} \|T'_i\|^2_{L^2(\hat{\gamma})} \leq \pi_1^2\, \bar{\xi}_1\, m^3 \|\boldsymbol{\tau}_m\|^2_{L^2(\hat{\gamma})}
\end{aligned}$$

where representation $(23)_1$ for $\boldsymbol{\tau}_m$, the bound in $(19)_3$, the Cauchy-Schwarz inequality and the upper bound in (27) have been employed. The Rayleigh quotient definition and the norm equivalence in $(24)_1$ conclude the proof of (29).
By exploiting the difference in the definitions of $\mathbf{A}^{1,0}$ and $\mathbf{A}^{0,1}$, we can derive result (30). Thus, after defining vector $\mathbf{y} = \mathbf{A}^{0,1}\mathbf{t}$ with

$$\mathbf{y}_i = \sum_{k=1}^{m} \int_{\hat{\gamma}} \mathbf{t}_k T'_k(\hat{x}_2)\ T_i(\hat{x}_2)\ \mathcal{M}_{12}(\boldsymbol{\Phi}(\hat{\mathbf{z}}))j(\hat{\mathbf{z}})\, d\hat{x}_2,$$

we obtain

$$\begin{aligned}
\mathbf{y}^T\mathbf{y} &= \sum_{i=1}^{m} \left[\sum_{k=1}^{m} \int_{\hat{\gamma}} \mathbf{t}_k T'_k(\hat{x}_2)\ T_i(\hat{x}_2)\ \mathcal{M}_{12}(\boldsymbol{\Phi}(\hat{\mathbf{z}}))j(\hat{\mathbf{z}})\, d\hat{x}_2 \right]^2 \\
&= \sum_{i=1}^{m} \left[\int_{\hat{\gamma}} \boldsymbol{\tau}'_m(\hat{x}_2)\ T_i(\hat{x}_2)\ \mathcal{M}_{12}(\boldsymbol{\Phi}(\hat{\mathbf{z}}))j(\hat{\mathbf{z}})\, d\hat{x}_2 \right]^2 \\
&\leq \pi_1^2 \|\boldsymbol{\tau}'_m\|^2_{L^2(\hat{\gamma})} \sum_{i=1}^{m} \|T_i\|^2_{L^2(\hat{\gamma})} \leq \pi_1^2\, \bar{\xi}_1\, m^3 \|\boldsymbol{\tau}_m\|^2_{L^2(\hat{\gamma})},
\end{aligned}$$

where we have used the representation for $\boldsymbol{\tau}'_m$ according to $(23)_1$, the bound in $(19)_3$, the Cauchy–Schwarz inequality, the inverse-type relation in (26) to bound

$\|\boldsymbol{\tau}'_m\|_{L^2(\hat{\gamma})}$ and the orthonormality assumption on modal functions T_i in (A1). Finally, result (30) follows from the Rayleigh quotient definition and the norm equivalence in $(24)_1$. □

The continuity and the inf-sup properties of the bilinear form $\tilde{b}(\cdot,\cdot)$ rely on the following result.

Lemma 4. *Under assumptions (A1), (A2) and (A3), we can prove the following inequalities*

1. *the spectral norm of the block matrices of functions* $\mathbf{B}^{0,0}$ *and* $\mathbf{B}^{1,0}$ *can be upper-bounded as*

$$\|\mathbf{B}^{0,0}\|_2^2 = \lambda_{\max}\big([\mathbf{B}^{0,0}]^T\mathbf{B}^{0,0}\big) \leq \gamma_{\max}^2\, m \qquad \forall \hat{x}_1 \in \hat{\Omega}_{1D}, \tag{31}$$

$$\|\mathbf{B}^{1,0}\|_2^2 = \lambda_{\max}\big([\mathbf{B}^{1,0}]^T\mathbf{B}^{1,0}\big) \leq \sigma_{\max}^2\, \bar{\xi}_1 m^3 \qquad \forall \hat{x}_1 \in \hat{\Omega}_{1D}, \tag{32}$$

   where $\gamma_{\max} = \max(\gamma_1, \gamma_2)$, $\sigma_{\max} = \max(\sigma_1, \sigma_2)$ *with* γ_1, γ_2, σ_1, σ_2 *defined as in* (20), *and where* $\bar{\xi}_1$ *is defined as in (A3);*

2. *the spectral norm of the block matrices of functions* $\big[\mathbf{B}^{0,0}\big]^T$ *and* $\big[\mathbf{B}^{1,0}\big]^T$ *can be bounded from above as*

$$\big\|\big[\mathbf{B}^{0,0}\big]^T\big\|_2^2 = \lambda_{\max}\big(\mathbf{B}^{0,0}\big[\mathbf{B}^{0,0}\big]^T\big) \leq \gamma_{\max}^2\, n \qquad \forall \hat{x}_1 \in \hat{\Omega}_{1D}, \tag{33}$$

$$\big\|\big[\mathbf{B}^{1,0}\big]^T\big\|_2^2 = \lambda_{\max}\big(\mathbf{B}^{1,0}\big[\mathbf{B}^{1,0}\big]^T\big) \leq \sigma_{\max}^2\, \bar{\xi}_1\, n\, m^2 \qquad \forall \hat{x}_1 \in \hat{\Omega}_{1D}. \tag{34}$$

Proof. The bound in (31) can be proved by defining vector $\mathbf{y} = [\mathbf{y}_1, \mathbf{y}_2, \ldots, \mathbf{y}_m]^T = \mathbf{B}^{0,0}\mathbf{r}$, with $\mathbf{r} = [r_1, \ldots, r_n]^T$ a generic vector in $\mathbb{R}^n$, being

$$\mathbf{y}_i = [y_{i,1}, y_{i,2}]^T = \sum_{l=1}^{n} \int_{\hat{\gamma}} r_l R_l(\hat{x}_2) T_i(\hat{x}_2)\, J_{(1,:)}(\boldsymbol{\Phi}(\hat{\mathbf{z}}))j(\hat{\mathbf{z}})\, d\hat{x}_2$$

for $i = 1, \ldots, m$, and $J_{(1,:)} = [J_{11}, J_{12}]^T$ the vector collecting the entries of the first row of the Jacobian in (3). Thus, we have

$$\mathbf{y}^T\mathbf{y} \;=\; \sum_{i=1}^{m} \left[\sum_{l=1}^{n} \int_{\hat{\gamma}} r_l R_l(\hat{x}_2) T_i(\hat{x}_2)\, J_{(1,:)}(\boldsymbol{\Phi}(\hat{\mathbf{z}}))j(\hat{\mathbf{z}})\, d\hat{x}_2 \right]^2$$

namely, thanks to the representation in $(23)_2$,

$$\begin{aligned} \mathbf{y}^T\mathbf{y} \;&=\; \sum_{i=1}^{m} \left[\int_{\hat{\gamma}} \rho_n(\hat{x}_2) T_i(\hat{x}_2)\, J_{(1,:)}(\boldsymbol{\Phi}(\hat{\mathbf{z}}))j(\hat{\mathbf{z}})\, d\hat{x}_2 \right]^2 \\ &\leq\; \gamma_{\max}^2\, \|\rho_n\|_{L^2(\hat{\gamma})}^2 \sum_{i=1}^{m} \|T_i\|_{L^2(\hat{\gamma})}^2 \leq \gamma_{\max}^2\, m\, \|\rho_n\|_{L^2(\hat{\gamma})}^2 = \gamma_{\max}^2\, m\, \|\mathbf{r}\|^2 \end{aligned}$$

where the upper bounds in the last row are due to $(20)_1$, for $s = 1, 2$, the Cauchy-Schwarz inequality, the assumption in (A1) and the norm equivalence in $(24)_2$. By resorting to the Rayleigh quotient definition, we get the desired

estimate.
To prove (33) we set $\mathbf{y} = [y_1, y_2, \dots, y_n]^T = \left[\mathbf{B}^{0,0}\right]^T \mathbf{t}$, with $\mathbf{t} = [\mathbf{t}_1, \mathbf{t}_2, \dots, \mathbf{t}_m]^T \in \mathbb{R}^{2m}$ and $\mathbf{t}_i = [t_{i,1}, t_{i,2}]^T$, so that

$$y_l = \sum_{i=1}^{m} \int_{\hat{\gamma}} R_l(\hat{x}_2)\, T_i(\hat{x}_2)\, \left[J_{(1,:)}(\mathbf{\Phi}(\hat{\mathbf{z}}))\right]^T \mathbf{t}_i\, j(\hat{\mathbf{z}})\, d\hat{x}_2$$

for $l = 1, \dots, n$. It follows

$$\begin{aligned} \mathbf{y}^t\mathbf{y} &= \sum_{l=1}^{n} \left[\int_{\hat{\gamma}} \boldsymbol{\tau}_m(\hat{x}_2) R_l(\hat{x}_2)\, \left[J_{(1,:)}(\mathbf{\Phi}(\hat{\mathbf{z}}))\right]^T j(\hat{\mathbf{z}})\, d\hat{x}_2 \right]^2 \\ &\leq \gamma_{\max}^2 \, \|\boldsymbol{\tau}_m\|^2_{L^2(\hat{\gamma})} \sum_{l=1}^{n} \|R_l\|^2_{L^2(\hat{\gamma})} \leq \gamma_{\max}^2\, n\, \|\boldsymbol{\tau}_m\|^2_{L^2(\hat{\gamma})} = \gamma_{\max}^2\, n\, \|\mathbf{t}\|^2 \end{aligned}$$

where we have employed the definition of $\boldsymbol{\tau}_m$ in $(23)_1$ in combination with the Cauchy-Schwarz inequality, the estimates for the Jacobian components in $(20)_1$, the orthonormality assumption (A2), and the equality in $(24)_1$. The definition of the Rayleigh quotient provides the desired result.
The bound in (32) can be proved by defining vector $\mathbf{y} = [\mathbf{y}_1, \mathbf{y}_2, \dots \mathbf{y}_m]^T = \mathbf{B}^{1,0}\mathbf{r}$, with $\mathbf{r} = [r_1, \dots, r_n]^T$ a generic vector in $\mathbb{R}^n$, being

$$\mathbf{y}_i = [y_{i,1}, y_{i,2}]^T = \sum_{l=1}^{n} \int_{\hat{\gamma}} r_l R_l(\hat{x}_2) T_i'(\hat{x}_2)\, J_{(2,:)}(\mathbf{\Phi}(\hat{\mathbf{z}})) j(\hat{\mathbf{z}})\, d\hat{x}_2$$

for $i = 1, \dots, m$, and vector $J_{(2,:)} = [J_{21}, J_{22}]^T$ which gathers the entries in the second row of the Jacobian (3). Thus, we have

$$\mathbf{y}^T\mathbf{y} = \sum_{i=1}^{m} \left[\sum_{l=1}^{n} \int_{\hat{\gamma}} r_l R_l(\hat{x}_2) T_i'(\hat{x}_2)\, J_{(2,:)}(\mathbf{\Phi}(\hat{\mathbf{z}})) j(\hat{\mathbf{z}})\, d\hat{x}_2 \right]^2$$

namely, using the modal expansion in $(23)_2$,

$$\begin{aligned} \mathbf{y}^T\mathbf{y} &= \sum_{i=1}^{m} \left[\int_{\hat{\gamma}} \rho_n(\hat{x}_2) T_i'(\hat{x}_2)\, J_{(2,:)}(\mathbf{\Phi}(\hat{\mathbf{z}})) j(\hat{\mathbf{z}})\, d\hat{x}_2 \right]^2 \\ &\leq \sigma_{\max}^2 \, \|\rho_n\|^2_{L^2(\hat{\gamma})} \sum_{i=1}^{m} \|T_i'\|^2_{L^2(\hat{\gamma})} \leq \sigma_{\max}^2\, \bar{\xi}_1\, m^3\, \|\rho_n\|^2_{L^2(\hat{\gamma})} \end{aligned}$$

where we have exploited relations in $(20)_2$, the Cauchy-Schwarz inequality and the upper bound in (27), thanks to assumptions (A1) and (A3). By resorting to the equivalence in $(24)_2$ and to the Rayleigh quotient definition, we have estimate (32).
To prove (34), we introduce vector $\mathbf{y} = [y_1, y_2, \dots, y_n]^T = \left[\mathbf{B}^{1,0}\right]^T \mathbf{t}$, being $\mathbf{t} = [\mathbf{t}_1, \mathbf{t}_2, \dots, \mathbf{t}_m]^T \in \mathbb{R}^{2m}$ and $\mathbf{t}_i = [t_{i,1}, t_{i,2}]^T$. It holds that

$$y_l = \sum_{i=1}^{m} \int_{\hat{\gamma}} R_l(\hat{x}_2) T_i'(\hat{x}_2)\, \left[J_{(2,:)}(\mathbf{\Phi}(\hat{\mathbf{z}}))\right]^T \mathbf{t}_i\, j(\hat{\mathbf{z}})\, d\hat{x}_2$$

for $l = 1, \dots, n$, so that

$$\mathbf{y}^t\mathbf{y} = \sum_{l=1}^{n} \left[\int_{\hat{\gamma}} \boldsymbol{\tau}'_m(\hat{x}_2) R_l(\hat{x}_2)\, \left[J_{(2,:)}(\mathbf{\Phi}(\hat{\mathbf{z}}))\right]^T j(\hat{\mathbf{z}})\, d\hat{x}_2 \right]^2 .$$

Thus, we have

$$\mathbf{y}^t\mathbf{y} \leq \sigma_{\max}^2 \|\boldsymbol{\tau}'_m\|^2_{L^2(\hat{\gamma})} \sum_{l=1}^{n} \|R_l\|^2_{L^2(\hat{\gamma})} \leq \sigma_{\max}^2\, n\, \bar{\xi}_1 m^2 \|\boldsymbol{\tau}_m\|^2_{L^2(\hat{\gamma})},$$

thanks to the definition of $\boldsymbol{\tau}'_m$ according to $(23)_1$, the upper bounds in $(20)_2$, the Cauchy-Schwarz inequality, assumption (A2) and the inverse-type estimate in (26). □

We now have all the necessary tools to address the well-posedness analysis of problem (7).

4 Well-posedness of the HiMod formulation

This section represents the core of the paper, where we establish the well-posedness of the HiMod discretization (7) for the Stokes problem, by customizing the standard inf-sup theory for saddle-point problems to the HiMod setting. The focus will be on the discretization along the transverse direction, to determine whether specific combinations of the modal indices, m and n, for the reduced velocity and pressure, respectively may influence the stability of the HiMod formulation. In contrast, along the supporting fiber we do not expect significant deviations from the standard inf-sup theory which properly relates the finite element spaces for velocity and pressure. This ansatz will be corroborated by the numerical assessment in Sec. 5.

The results from the previous section, along with the compact notation introduced in (16), will play a fundamental role in the proof of the main theorem of this section, namely

Theorem 5. *We assume that hypotheses (A1), (A2), (A3), (A4) hold. In addition, we require that the constant π_1 in $(19)_3$ is a $O(m^{-3/2})$, while the constant σ_1 in $(20)_2$ is a $O(n^{-3/2})$ and that $m \geq n$. Then, there exists a unique HiMod pair $(\hat{\mathbf{U}}_m, \hat{\mathbf{P}}_n) \in \mathbb{V}_{m,x} \times \mathbb{Q}_{n,x}$ solution to (16) that satisfies the stability estimates*

$$\|\hat{\mathbf{U}}_m\|_{\mathbb{V}_{m,x}} \leq \frac{M_F}{\alpha}, \qquad \|\hat{\mathbf{P}}_n\|_{\mathbb{Q}_{n,x}} \leq \frac{1}{\beta}\left(1 + \frac{M_a}{\alpha}\right) M_F \tag{35}$$

where:

$$M_F = M_F(m) = j_1^{\frac{1}{2}}\, m^{\frac{1}{2}}\, \|\mathbf{f}\|_{L^2(\Omega)}$$

is the continuity constant of the linear form $\tilde{F}(\cdot)$ in $(17)_4$, with j_1 the upper bound in (18);

$$\alpha = \alpha(m) = \frac{\nu}{2}\left\{\vartheta_0 + \xi_0\, \bar{\xi}_0 + \left[\left(\xi_0\, \bar{\xi}_0 - \vartheta_0\right)^2 + 4\,\pi_1^2\, \bar{\xi}_1\, m^3\right]^{\frac{1}{2}}\right\}$$

the coercivity constant of the bilinear form $\tilde{a}(\cdot,\cdot)$ in $(17)_1$, with ϑ_0 and ξ_0 the constants involved in the regularity assumptions in (19) on map $\boldsymbol{\Psi}$, $\bar{\xi}_0$, $\bar{\xi}_1$ the constants characterizing the lower and the upper bound in hypothesis (A3);

$$\beta = \beta(n) = \left\{\left[\frac{2\, n^{\frac{1}{4}}}{\gamma_0^2}\, \sigma_1^2\, \bar{\xi}_1\, n^3 + 1\right] \kappa_0 + \frac{2\, n^{\frac{1}{4}}}{\gamma_0^2}\right\}^{-\frac{1}{2}}$$

the inf-sup constant for the bilinear form $\tilde{b}(\cdot,\cdot)$ *in* (17)$_3$*, with* γ_0 *defined as in (A4),*

$$\kappa_0(n) = \frac{n^{\frac{1}{8}}}{4\,\varepsilon\,\gamma_0}\left\{\frac{1}{2} - \frac{n^{\frac{1}{8}}}{\gamma_0}\left[\sigma_1\,(\bar{\xi}_1)^{\frac{1}{2}}\,n^{\frac{3}{2}} + \varepsilon\right]\right\}^{-1},$$

with ε *an arbitrary positive constant such that inequality* $\varepsilon < \gamma_0/(2\,n^{\frac{1}{8}})$ *holds;*

$$M_a = M_a(m) = \nu\,\left[\vartheta_1 + \xi_1\,\bar{\xi}_1\,m^2 + 2\,\pi_1\,(\bar{\xi}_1)^{\frac{1}{2}}\,m^{\frac{3}{2}}\right],$$

the continuity constant of the bilinear form $\tilde{a}(\cdot,\cdot)$*, with* ϑ_1 *and* ξ_1 *the constants appearing in the regularity assumptions* (19) *on the map* $\boldsymbol{\Psi}$*.*

Proof. According to the standard theory in [28], we proceed by establishing the continuity and coercivity of $\tilde{a}(\cdot,\cdot)$, the continuity and the inf-sup condition of $\tilde{b}(\cdot,\cdot)$ and the continuity of $\tilde{F}$. Each of these properties is analyzed separately in the following.

Continuity of $\tilde{a}(\cdot,\cdot)$ We aim to prove the existence of a constant $M_a > 0$ such that

$$\left|\tilde{a}(\hat{\mathbf{U}}_m, \hat{\mathbf{W}}_m)\right| \leq M_a\,\|\hat{\mathbf{U}}_m\|_{\mathbb{V}_{m,x}}\,\|\hat{\mathbf{W}}_m\|_{\mathbb{V}_{m,x}} \qquad \forall \hat{\mathbf{U}}_m, \hat{\mathbf{W}}_m \in \mathbb{V}_{m,x}, \tag{36}$$

with $\mathbb{V}_{m,x} \equiv H^1_{\{0\}}(\hat{\Omega}_{1D};\,\mathbb{R}^{2m})$. We bound the four terms on the right-hand side of (17)$_1$, separately. In particular, we employ the compatibility between the spectral and the Euclidean norms, Lemma 3, the Cauchy-Schwarz inequality and the standard relation between the $L^2(\hat{\Omega}_{1D})$- and the $H^1(\hat{\Omega}_{1D})$-norms, to obtain

$$\begin{aligned}
&\left|\nu\int_{\hat{\Omega}_{1D}}\left[\hat{\mathbf{W}}'_m\right]^T\mathbf{A}^{0,0}\,\hat{\mathbf{U}}'_m\,d\hat{x}_1\right| \leq \nu\int_{\hat{\Omega}_{1D}}\|\hat{\mathbf{W}}'_m\|\,\|\mathbf{A}^{0,0}\|_2\,\|\hat{\mathbf{U}}'_m\|\,d\hat{x}_1\\
=\;& \nu\int_{\hat{\Omega}_{1D}}\lambda_{\max}(\mathbf{A}^{0,0})\,\|\hat{\mathbf{W}}'_m\|\,\|\hat{\mathbf{U}}'_m\|\,d\hat{x}_1 \leq \nu\,\vartheta_1\int_{\hat{\Omega}_{1D}}\|\hat{\mathbf{W}}'_m\|\,\|\hat{\mathbf{U}}'_m\|\,d\hat{x}_1\\
\leq\;& \nu\,\vartheta_1\,\|\hat{\mathbf{W}}'_m\|_{L^2(\hat{\Omega}_{1D};\,\mathbb{R}^{2m})}\,\|\hat{\mathbf{U}}'_m\|_{L^2(\hat{\Omega}_{1D};\,\mathbb{R}^{2m})} \leq \nu\,\vartheta_1\,\|\hat{\mathbf{W}}_m\|_{\mathbb{V}_{m,x}}\,\|\hat{\mathbf{U}}_m\|_{\mathbb{V}_{m,x}}.
\end{aligned}$$

In a similar way, we have

$$\begin{aligned}
&\left|\nu\int_{\hat{\Omega}_{1D}}\left[\hat{\mathbf{W}}_m\right]^T\mathbf{A}^{1,1}\,\hat{\mathbf{U}}_m\,d\hat{x}_1\right| \leq \nu\int_{\hat{\Omega}_{1D}}\|\hat{\mathbf{W}}_m\|\,\|\mathbf{A}^{1,1}\|_2\,\|\hat{\mathbf{U}}_m\|\,d\hat{x}_1\\
\leq\;& \nu\,\xi_1\,\bar{\xi}_1\,m^2\int_{\hat{\Omega}_{1D}}\|\hat{\mathbf{W}}_m\|\,\|\hat{\mathbf{U}}_m\|\,d\hat{x}_1 \leq \nu\,\xi_1\,\bar{\xi}_1\,m^2\,\|\hat{\mathbf{W}}_m\|_{\mathbb{V}_{m,x}}\,\|\hat{\mathbf{U}}_m\|_{\mathbb{V}_{m,x}}.
\end{aligned}$$

Concerning the non-symmetric contributions, it follows

$$\begin{aligned}
&\left|\nu\int_{\hat\Omega_{1D}}\left[\hat{\mathbf{W}}_m\right]^T\mathbf{A}^{1,0}\,\hat{\mathbf{U}}'_m\,d\hat x_1\right| \le \nu\int_{\hat\Omega_{1D}}\|\hat{\mathbf{W}}_m\|\,\|\mathbf{A}^{1,0}\|_2\,\|\hat{\mathbf{U}}'_m\|\,d\hat x_1\\
=\;&\nu\int_{\hat\Omega_{1D}}\left(\lambda_{\max}([\mathbf{A}^{1,0}]^T\mathbf{A}^{1,0})\right)^{\frac12}\|\hat{\mathbf{W}}_m\|\,\|\hat{\mathbf{U}}'_m\|\,d\hat x_1\\
\le\;&\nu\,\pi_1\,(\bar\xi_1)^{\frac12}\,m^{\frac32}\int_{\hat\Omega_{1D}}\|\hat{\mathbf{W}}_m\|\,\|\hat{\mathbf{U}}'_m\|\,d\hat x_1\\
\le\;&\nu\,\pi_1\,(\bar\xi_1)^{\frac12}\,m^{\frac32}\,\|\hat{\mathbf{W}}_m\|_{L^2(\hat\Omega_{1D};\mathbb{R}^{2m})}\,\|\hat{\mathbf{U}}'_m\|_{L^2(\hat\Omega_{1D};\mathbb{R}^{2m})}\\
\le\;&\nu\,\pi_1\,(\bar\xi_1)^{\frac12}\,m^{\frac32}\,\|\hat{\mathbf{W}}_m\|_{\mathbb{V}_{m,x}}\,\|\hat{\mathbf{U}}_m\|_{\mathbb{V}_{m,x}},
\end{aligned}$$

and

$$\begin{aligned}
\left|\nu\int_{\hat\Omega_{1D}}\left[\hat{\mathbf{W}}'_m\right]^T\mathbf{A}^{0,1}\,\hat{\mathbf{U}}_m\,d\hat x_1\right| &\le \nu\int_{\hat\Omega_{1D}}\|\hat{\mathbf{W}}'_m\|\,\|\mathbf{A}^{0,1}\|_2\,\|\hat{\mathbf{U}}_m\|\,d\hat x_1\\
&\le \nu\,\pi_1\,(\bar\xi_1)^{\frac12}\,m^{\frac32}\int_{\hat\Omega_{1D}}\|\hat{\mathbf{W}}'_m\|\,\|\hat{\mathbf{U}}_m\|\,d\hat x_1\\
&\le \nu\,\pi_1\,(\bar\xi_1)^{\frac12}\,m^{\frac32}\,\|\hat{\mathbf{W}}_m\|_{\mathbb{V}_{m,x}}\,\|\hat{\mathbf{U}}_m\|_{\mathbb{V}_{m,x}},
\end{aligned}$$

respectively. This concludes the proof of (36) with $M_a = \nu\left[\vartheta_1 + \xi_1\,\bar\xi_1\,m^2 + 2\,\pi_1\,(\bar\xi_1)^{\frac12}\,m^{\frac32}\right]$.

Coercivity of $\tilde a(\cdot,\cdot)$ We look for a constant $\alpha>0$ such that

$$\tilde a(\hat{\mathbf{U}}_m,\hat{\mathbf{U}}_m) \ge \alpha\,\|\hat{\mathbf{U}}_m\|^2_{\mathbb{V}_{m,x}} \qquad \forall\hat{\mathbf{U}}_m\in\mathbb{V}_{m,x}. \tag{37}$$

We start by considering the contributions in $(17)_1$ associated with the symmetric positive definite matrices $\mathbf{A}^{0,0}$ and $\mathbf{A}^{1,1}$. Thanks to the Rayleigh quotient definition and Lemma 3, it holds

$$\begin{aligned}
&\nu\int_{\hat\Omega_{1D}}\left\{\left[\hat{\mathbf{U}}'_m\right]^T\mathbf{A}^{0,0}\,\hat{\mathbf{U}}'_m + \left[\hat{\mathbf{U}}_m\right]^T\mathbf{A}^{1,1}\,\hat{\mathbf{U}}_m\right\}d\hat x_1\\
\ge\;&\nu\,\lambda_{\min}(\mathbf{A}^{0,0})\int_{\hat\Omega_{1D}}\|\hat{\mathbf{U}}'_m\|^2\,d\hat x_1 + \nu\,\lambda_{\min}(\mathbf{A}^{1,1})\int_{\hat\Omega_{1D}}\|\hat{\mathbf{U}}_m\|^2\,d\hat x_1\\
\ge\;&\nu\,\vartheta_0\,\|\hat{\mathbf{U}}'_m\|^2_{L^2(\hat\Omega_{1D};\mathbb{R}^{2m})} + \nu\,\xi_0\,\bar\xi_0\,\|\hat{\mathbf{U}}_m\|^2_{L^2(\hat\Omega_{1D};\mathbb{R}^{2m})}.
\end{aligned}$$

By adding the terms involving matrices $\mathbf{A}^{1,0}$ and $\mathbf{A}^{0,1}$ after observing that $[\hat{\mathbf{U}}_m]^T\mathbf{A}^{1,0}\,\hat{\mathbf{U}}'_m = [\hat{\mathbf{U}}'_m]^T\mathbf{A}^{0,1}\,\hat{\mathbf{U}}_m$, we have

$$\begin{aligned}
&\tilde a(\hat{\mathbf{U}}_m,\hat{\mathbf{U}}_m) \ge \nu\,\vartheta_0\,\|\hat{\mathbf{U}}'_m\|^2_{L^2(\hat\Omega_{1D};\mathbb{R}^{2m})} + \nu\,\xi_0\,\bar\xi_0\,\|\hat{\mathbf{U}}_m\|^2_{L^2(\hat\Omega_{1D};\mathbb{R}^{2m})}\\
+\;&2\,\nu\int_{\hat\Omega_{1D}}\left[\hat{\mathbf{U}}_m\right]^T\mathbf{A}^{1,0}\,\hat{\mathbf{U}}'_m\,d\hat x_1 \ge \nu\left(\xi_0\,\bar\xi_0 - \frac{1}{2\,\varepsilon}\right)\|\hat{\mathbf{U}}_m\|^2_{L^2(\hat\Omega_{1D};\mathbb{R}^{2m})}\\
+\;&\nu\left(\vartheta_0 - 2\,\varepsilon\,\pi_1^2\,\bar\xi_1\,m^3\right)\|\hat{\mathbf{U}}'_m\|^2_{L^2(\hat\Omega_{1D};\mathbb{R}^{2m})},
\end{aligned} \tag{38}$$

where the last inequality follows from Young's inequality and Lemma 3, with $\varepsilon > 0$ to be properly selected. In particular, we choose ε to ensure that both the quantities in brackets are strictly positive and, additionally, to arbitrarily enforce that the coefficient multiplying the norm of $\hat{\mathbf{U}}_m$ is greater than $\|\hat{\mathbf{U}}'_m\|_{L^2(\hat{\Omega}_{1D};\mathbb{R}^{2m})}$. This implies that

$$0 < \vartheta_0 - 2\,\varepsilon\,\pi_1^2\,\bar{\xi}_1\,m^3 < \xi_0\,\bar{\xi}_0 - \frac{1}{2\,\varepsilon}. \tag{39}$$

The left inequality requires that $0 < \varepsilon < \varepsilon^*$ with $\varepsilon^* = \vartheta_0 \big(2\,\pi_1^2\,\bar{\xi}_1\,m^3\big)^{-1}$. The right inequality leads to demand that $\varepsilon < \tilde{\varepsilon}_0$ as well as $\varepsilon > \tilde{\varepsilon}_1$ with

$$\tilde{\varepsilon}_{0,1} = \frac{\vartheta_0 - \xi_0\,\bar{\xi}_0 \pm \Big[\big(\xi_0\,\bar{\xi}_0 - \vartheta_0\big)^2 + 4\,\pi_1^2\,\bar{\xi}_1\,m^3\Big]^{\frac{1}{2}}}{4\,\pi_1^2\,\bar{\xi}_1\,m^3}.$$

We observe that $\tilde{\varepsilon}_0 < \tilde{\varepsilon}_1$, regardless of the sign taken by the quantity $\vartheta_0 - \xi_0\,\bar{\xi}_0$. Now, to simultaneously satisfy the two requirements on ε, we have to prescribe that $\tilde{\varepsilon}_1 < \varepsilon^*$, namely we have to assume that

$$\pi_1^2 < \frac{\vartheta_0\,\xi_0\,\bar{\xi}_0}{\bar{\xi}_1\,m^3}. \tag{40}$$

This allows us to arbitrarily choose parameter ε in (38) as $\bar{\varepsilon}$ in the interval $(\tilde{\varepsilon}_1, \varepsilon^*)$, where the optimal choice is $\bar{\varepsilon} = \tilde{\varepsilon}_1$. This leads us to the inequality

$$\tilde{a}(\hat{\mathbf{U}}_m, \hat{\mathbf{U}}_m) \geq \nu\,\frac{\vartheta_0 + \xi_0\,\bar{\xi}_0 + \Big[\big(\xi_0\,\bar{\xi}_0 - \vartheta_0\big)^2 + 4\,\pi_1^2\,\bar{\xi}_1\,m^3\Big]^{\frac{1}{2}}}{2}\,\|\hat{\mathbf{U}}_m\|^2_{\mathbb{V}_{m,x}},$$

namely to inequality (37) with $\alpha = \frac{\nu}{2}\Big\{\vartheta_0 + \xi_0\,\bar{\xi}_0 + \Big[\big(\xi_0\,\bar{\xi}_0 - \vartheta_0\big)^2 + 4\,\pi_1^2\,\bar{\xi}_1\,m^3\Big]^{\frac{1}{2}}\Big\}$, thus proving the coercivity of $\tilde{a}(\cdot,\cdot)$.[2]

Continuity of $\tilde{b}(\cdot,\cdot)$ The objective is to prove the existence of a constant $M_b > 0$ such that

$$\big|\tilde{b}(\hat{\mathbf{U}}_m, \hat{\mathbf{Z}}_n)\big| \leq M_b\,\|\hat{\mathbf{U}}_m\|_{\mathbb{V}_{m,x}}\,\|\hat{\mathbf{Z}}_n\|_{\mathbb{Q}_{n,x}} \qquad \forall \hat{\mathbf{U}}_m \in \mathbb{V}_{m,x} \text{ and } \forall \hat{\mathbf{Z}}_n \in \mathbb{Q}_{n,x}, \tag{41}$$

with $\mathbb{Q}_{n,x} \equiv L^2(\hat{\Omega}_{1D};\,\mathbb{R}^n)$. Starting from definition $(17)_3$, we leverage the compatibility between the spectral and the Euclidean norms, Lemma 4, the Cauchy-Schwarz inequality and the standard relation between the $L^2(\hat{\Omega}_{1D})$- and the

[2] Inequalities alternative to (39) could be used to prove the coercivity of the bilinear form $\tilde{a}(\cdot,\cdot)$. For instance, we can impose that

$$0 < \xi_0\,\bar{\xi}_0 - \frac{1}{2\,\varepsilon} < \vartheta_0 - 2\,\varepsilon\,\pi_1^2\,\bar{\xi}_1\,m^3$$

or $\vartheta_0 - 2\,\varepsilon\,\pi_1^2\,\bar{\xi}_1\,m^3 > 0$ and $\bar{\xi}_0 - \big(2\,\varepsilon\big)^{-1} > 0$, separately. It is worth noting that these different requirements lead to the same relationship between π_1 and the modal index m as in (40), although the coercivity constant α in (37) may vary.

$H^1(\hat{\Omega}_{1D})$-norms. This yields the sequence of inequalities

$$\begin{aligned}
\left|\tilde{b}(\hat{\mathbf{U}}_m, \hat{\mathbf{Z}}_n)\right| &\leq \left| \int_{\hat{\Omega}_{1D}} \left[\hat{\mathbf{Z}}_n\right]^T \left[\mathbf{B}^{0,0}\right]^T \hat{\mathbf{U}}'_m \, d\hat{x}_1 \right| + \left| \int_{\hat{\Omega}_{1D}} \left[\hat{\mathbf{Z}}_n\right]^T \left[\mathbf{B}^{1,0}\right]^T \hat{\mathbf{U}}_m \, d\hat{x}_1 \right| \\
&\leq \int_{\hat{\Omega}_{1D}} \|\hat{\mathbf{Z}}_n\| \, \|[\mathbf{B}^{0,0}]^T\|_2 \, \|\hat{\mathbf{U}}'_m\| \, d\hat{x}_1 + \int_{\hat{\Omega}_{1D}} \|\hat{\mathbf{Z}}_n\| \, \|[\mathbf{B}^{1,0}]^T\|_2 \, \|\hat{\mathbf{U}}_m\| \, d\hat{x}_1 \\
&\leq \gamma_{\max} \, n^{\frac{1}{2}} \, \|\hat{\mathbf{Z}}_n\|_{L^2(\hat{\Omega}_{1D};\mathbb{R}^n)} \, \|\hat{\mathbf{U}}'_m\|_{L^2(\hat{\Omega}_{1D};\mathbb{R}^{2m})} \\
&+ \sigma_{\max} \, (\bar{\xi}_1)^{\frac{1}{2}} \, n^{\frac{1}{2}} \, m \, \|\hat{\mathbf{Z}}_n\|_{L^2(\hat{\Omega}_{1D};\mathbb{R}^n)} \, \|\hat{\mathbf{U}}_m\|_{L^2(\hat{\Omega}_{1D};\mathbb{R}^{2m})} \\
&\leq n^{\frac{1}{2}} \left[\gamma_{\max} + \sigma_{\max} \, (\bar{\xi}_1)^{\frac{1}{2}} \, m\right] \|\hat{\mathbf{Z}}_n\|_{\mathbb{Q}_{n,x}} \, \|\hat{\mathbf{U}}_m\|_{\mathbb{V}_{m,x}},
\end{aligned}$$

namely the desired result in (41) with $M_b = n^{\frac{1}{2}} \left[\gamma_{\max} + \sigma_{\max} \, (\bar{\xi}_1)^{\frac{1}{2}} \, m\right]$.

The inf-sup condition for $\tilde{b}(\cdot,\cdot)$ Our goal is to identify a constant $\beta = \beta(n) > 0$ such that

$$\inf_{\hat{\mathbf{Z}}_n \in \mathbb{Q}_{n,x}} \sup_{\hat{\mathbf{U}}_m \in \mathbb{V}_{m,x}} \tilde{b}(\hat{\mathbf{U}}_m, \hat{\mathbf{Z}}_n) \geq \beta \, \|\hat{\mathbf{U}}_m\|_{\mathbb{V}_{m,x}} \, \|\hat{\mathbf{Z}}_n\|_{\mathbb{Q}_{n,x}}. \tag{42}$$

This is equivalent to selecting an arbitrary pressure

$$\hat{\mathbf{Z}}^*_n = \hat{\mathbf{Z}}^*_n(\hat{x}_1) = [\hat{z}^*_1, \hat{z}^*_2, \ldots, \hat{z}^*_n]^T \in \mathbb{Q}_{n,x}$$

with $\hat{z}^*_l = \hat{z}^*_l(\hat{x}_1)$ for $l = 1, \ldots, n$, and accordingly identifying a velocity

$$\hat{\mathbf{U}}^*_m = \hat{\mathbf{U}}^*_m(\hat{x}_1) = [\hat{\mathbf{u}}^*_1, \hat{\mathbf{u}}^*_2, \ldots, \hat{\mathbf{u}}^*_m]^T \in \mathbb{V}_{m,x},$$

with $\hat{\mathbf{u}}^*_k = \hat{\mathbf{u}}^*_k(\hat{x}_1) = [\hat{u}^*_{k,1}(\hat{x}_1), \hat{u}^*_{k,2}(\hat{x}_1)]^T$ for $k = 1, \ldots, m$, that satisfies relations

$$\begin{aligned}
&\tilde{b}(\hat{\mathbf{U}}^*_m, \hat{\mathbf{Z}}^*_n) = \|\hat{\mathbf{Z}}^*_n\|^2_{\mathbb{Q}_{n,x}} \\
&\|\hat{\mathbf{U}}^*_m\|_{\mathbb{V}_{m,x}} \leq \kappa(n) \, \|\hat{\mathbf{Z}}^*_n\|_{\mathbb{Q}_{n,x}},
\end{aligned} \tag{43}$$

with $\kappa(n) > 0$ and where β in (42) depends on this constant. To build $\hat{\mathbf{U}}^*_m$, we begin by requiring that

$$\begin{aligned}
u^*_{k,2}(\hat{x}_1) = 0 \qquad & k = 1, \ldots, m, \\
u^*_{k,1}(\hat{x}_1) = 0 \qquad & k = n+1, \ldots, m,
\end{aligned}$$

having assumed that $m \geq n$. These assumptions lead us to introduce the condensed velocity vector $\hat{\mathbf{U}}^{*,c}_n = \hat{\mathbf{U}}^{*,c}_n(\hat{x}_1) = [\hat{u}^{*,c}_1, \hat{u}^{*,c}_2, \ldots, \hat{u}^{*,c}_n]^T \in \mathbb{V}^c_{n,x} = [\hat{V}^c_{1D}]^n$ with $\hat{V}^c_{1D} = \left\{\hat{v} \in H^1(\hat{\Omega}_{1D}) : \hat{v}(0) = 0\right\}$ and with $\hat{u}^{*,c}_k = \hat{u}^{*,c}_k(\hat{x}_1)$ for $k = 1, \ldots, n$. In practice, velocity $\hat{\mathbf{U}}^{*,c}_n$ is a 1D vector which gathers the non-null components of $\hat{\mathbf{U}}^*_m$, so that the bilinear form on the left-hand side of $(43)_1$ can be equivalently rewritten as

$$\begin{aligned}
\tilde{b}(\hat{\mathbf{U}}^*_m, \hat{\mathbf{Z}}^*_n) &= -\int_{\hat{\Omega}_{1D}} \left\{ \left[\hat{\mathbf{Z}}^*_n\right]^T \left[\mathbf{B}^{0,0}_c\right]^T \left[\hat{\mathbf{U}}^{*,c}_n\right]' + \left[\hat{\mathbf{Z}}^*_n\right]^T \left[\mathbf{B}^{1,0}_c\right]^T \hat{\mathbf{U}}^{*,c}_n \right\} d\hat{x}_1 \\
&:= \tilde{b}_n(\hat{\mathbf{U}}^{*,c}_n, \hat{\mathbf{Z}}^*_n),
\end{aligned}$$

where $\mathbf{B}_c^{0,0}$ is defined as in (22), while $\mathbf{B}_c^{1,0} = \mathbf{B}_c^{1,0}(\hat{x}_1)$ is the $n \times n$ block matrix of functions whose i-th row is defined by

$$\left[\mathbf{B}_c^{1,0}\right]_i = \left[\mathcal{B}_{i1,1}^{1,0}, \mathcal{B}_{i2,1}^{1,0}, \ldots, \mathcal{B}_{in,1}^{1,0}\right] \in \mathbb{R}^n. \tag{44}$$

Thus, to prove equality $(43)_1$, we have to ensure that

$$-\int_{\hat{\Omega}_{1D}} \left\{ \left[\hat{\mathbf{Z}}_n^*\right]^T \left[\mathbf{B}_c^{0,0}\right]^T \left[\hat{\mathbf{U}}_n^{*,c}\right]' + \left[\hat{\mathbf{Z}}_n^*\right]^T \left[\mathbf{B}_c^{1,0}\right]^T \hat{\mathbf{U}}_n^{*,c} \right\} d\hat{x}_1 = \int_{\hat{\Omega}_{1D}} \left[\hat{\mathbf{Z}}_n^*\right]^T \hat{\mathbf{Z}}_n^* \, d\hat{x}_1.$$

For this condition to hold, it is enough that

$$\left[\mathbf{B}_c^{0,0}\right]^T \left[\hat{\mathbf{U}}_n^{*,c}\right]' + \left[\mathbf{B}_c^{1,0}\right]^T \hat{\mathbf{U}}_n^{*,c} = -\hat{\mathbf{Z}}_n^*$$

for any $\hat{x}_1 \in \hat{\Omega}_{1D}$. Now, since $\hat{\mathbf{U}}_n^{*,c} \in \mathbb{V}_{n,x}^c$, it holds $\hat{\mathbf{U}}_n^{*,c}(0) = \mathbf{0}$, so that the velocity vector $\hat{\mathbf{U}}_n^{*,c}$ satisfies the Cauchy problem

$$\begin{cases} \left[\hat{\mathbf{U}}_n^{*,c}\right]' = -\left[\mathbf{B}_c^{0,0}\right]^{-T} \left[\mathbf{B}_c^{1,0}\right]^T \hat{\mathbf{U}}_n^{*,c} - \left[\mathbf{B}_c^{0,0}\right]^{-T} \hat{\mathbf{Z}}_n^* \\ \hat{\mathbf{U}}_n^{*,c}(0) = \mathbf{0} \end{cases} \tag{45}$$

for any $\hat{x}_1 \in \hat{\Omega}_{1D}$, where assumption (A4) guarantees the invertibility of matrix $\mathbf{B}_c^{0,0}$. Problem (45) admits a unique solution thanks to the regularity assumptions on maps $\boldsymbol{\Psi}$ and $\boldsymbol{\Phi}$. This proves equality $(43)_1$. Concerning result $(43)_2$, we first verify the two inequalities

$$\begin{aligned} \left\|\hat{\mathbf{U}}_n^{*,c}\right\|^2_{L^2(\hat{\Omega}_{1D};\mathbb{R}^n)} &\leq \kappa_0(n) \left\|\hat{\mathbf{Z}}_n^*\right\|^2_{L^2(\hat{\Omega}_{1D};\mathbb{R}^n)} \\ \left\|\left[\hat{\mathbf{U}}_n^{*,c}\right]'\right\|^2_{L^2(\hat{\Omega}_{1D};\mathbb{R}^n)} &\leq \kappa_1(n) \left\|\hat{\mathbf{Z}}_n^*\right\|^2_{L^2(\hat{\Omega}_{1D};\mathbb{R}^n)}, \end{aligned} \tag{46}$$

for some positive quantities $\kappa_0(n)$ and $\kappa_1(n)$. We start by proving $(46)_1$. To this aim, we multiply the differential equation in (45) by $\left[\hat{\mathbf{U}}_n^{*,c}\right]^T$ to obtain

$$\begin{aligned} \frac{1}{2}\frac{d\|\hat{\mathbf{U}}_n^{*,c}\|^2}{d\hat{x}_1} &= \left[\hat{\mathbf{U}}_n^{*,c}\right]^T \left[\hat{\mathbf{U}}_n^{*,c}\right]' \\ &= -\left[\hat{\mathbf{U}}_n^{*,c}\right]^T \left[\mathbf{B}_c^{0,0}\right]^{-T} \left[\mathbf{B}_c^{1,0}\right]^T \hat{\mathbf{U}}_n^{*,c} - \left[\hat{\mathbf{U}}_n^{*,c}\right]^T \left[\mathbf{B}_c^{0,0}\right]^{-T} \hat{\mathbf{Z}}_n^*. \end{aligned}$$

Thanks to the compatibility between the spectral and the Euclidean norms, it follows

$$\begin{aligned} \frac{1}{2}\frac{d\|\hat{\mathbf{U}}_n^{*,c}\|^2}{d\hat{x}_1} &\leq \left\|\left[\mathbf{B}_c^{0,0}\right]^{-T}\right\|_2 \left\|\left[\mathbf{B}_c^{1,0}\right]^T\right\|_2 \left\|\hat{\mathbf{U}}_n^{*,c}\right\|^2 + \left\|\left[\mathbf{B}_c^{0,0}\right]^{-T}\right\|_2 \|\hat{\mathbf{U}}_n^{*,c}\| \, \|\hat{\mathbf{Z}}_n^*\| \\ &= \left\|\left[\mathbf{B}_c^{0,0}\right]^{-1}\right\|_2 \left\|\mathbf{B}_c^{1,0}\right\|_2 \left\|\hat{\mathbf{U}}_n^{*,c}\right\|^2 + \left\|\left[\mathbf{B}_c^{0,0}\right]^{-1}\right\|_2 \|\hat{\mathbf{U}}_n^{*,c}\| \, \|\hat{\mathbf{Z}}_n^*\| \\ &\leq \frac{n^{\frac{1}{8}}}{\gamma_0} \sigma_1\left(\bar{\xi}_1\right)^{\frac{1}{2}} n^{\frac{3}{2}} \left\|\hat{\mathbf{U}}_n^{*,c}\right\|^2 + \frac{n^{\frac{1}{8}}}{\gamma_0} \|\hat{\mathbf{U}}_n^{*,c}\| \, \|\hat{\mathbf{Z}}_n^*\|, \end{aligned} \tag{47}$$

where the last inequality is due to assumption (A4) and to the counterpart of result (32) when applied to the condensed matrix in (44). By integrating on

$(0, \hat{x}_1)$ and using the Young inequality on the second term at the right-hand side, we have

$$\frac{1}{2}\,\|\hat{\mathbf{U}}_n^{*,c}(\hat{x}_1)\|^2 \leq \frac{n^{\frac{1}{8}}}{\gamma_0}\left[\sigma_1\,(\bar{\xi}_1)^{\frac{1}{2}}\,n^{\frac{3}{2}}+\varepsilon\right]\int_{\hat{\Omega}_{1D}}\left\|\hat{\mathbf{U}}_n^{*,c}\right\|^2 d\hat{x}_1+\frac{n^{\frac{1}{8}}}{4\,\varepsilon\,\gamma_0}\int_{\hat{\Omega}_{1D}}\|\hat{\mathbf{Z}}_n^*\|^2\,d\hat{x}_1$$
$$=\frac{n^{\frac{1}{8}}}{\gamma_0}\left[\sigma_1\,(\bar{\xi}_1)^{\frac{1}{2}}\,n^{\frac{3}{2}}+\varepsilon\right]\|\hat{\mathbf{U}}_n^{*,c}\|^2_{L^2(\hat{\Omega}_{1D};\mathbb{R}^n)}+\frac{n^{\frac{1}{8}}}{4\,\varepsilon\,\gamma_0}\,\|\hat{\mathbf{Z}}_n^*\|^2_{L^2(\hat{\Omega}_{1D};\mathbb{R}^n)}$$

being $\hat{\mathbf{U}}_n^{*,c}(0)=\mathbf{0}$ and with $\varepsilon>0$ to be properly selected. As a result of a further integration on $\hat{\Omega}_{1D}$, we find

$$\left\{\frac{1}{2}-\frac{n^{\frac{1}{8}}}{\gamma_0}\left[\sigma_1\,(\bar{\xi}_1)^{\frac{1}{2}}\,n^{\frac{3}{2}}+\varepsilon\right]\right\}\|\hat{\mathbf{U}}_n^{*,c}\|^2_{L^2(\hat{\Omega}_{1D};\mathbb{R}^n)}\leq\frac{n^{\frac{1}{8}}}{4\,\varepsilon\,\gamma_0}\,\|\hat{\mathbf{Z}}_n^*\|^2_{L^2(\hat{\Omega}_{1D};\mathbb{R}^n)},$$

namely relation $(46)_1$ after setting

$$\kappa_0(n)=\frac{n^{\frac{1}{8}}}{4\,\varepsilon\,\gamma_0}\left\{\frac{1}{2}-\frac{n^{\frac{1}{8}}}{\gamma_0}\left[\sigma_1\,(\bar{\xi}_1)^{\frac{1}{2}}\,n^{\frac{3}{2}}+\varepsilon\right]\right\}^{-1}.$$

To guarantee the positiveness of $\kappa_0(n)$, we require that

$$\sigma_1<\frac{\gamma_0-2\,n^{\frac{1}{8}}\,\varepsilon}{2\,(\bar{\xi}_1)^{\frac{1}{2}}\,n^{\frac{13}{8}}},\qquad \varepsilon<\frac{\gamma_0}{2\,n^{\frac{1}{8}}}.$$

We observe that the choice of ε is problem-dependent since, from the second bound above, it follows a request on the quantity $\gamma_0^2\,n^{-\frac{1}{4}}$ involved in assumption (A4)[3].

Result $(46)_2$ follows by exploiting similar computations as in (47), starting from the differential equation in $(45)_1$. Indeed, it holds

$$\begin{aligned}\|\left[\hat{\mathbf{U}}_n^{*,c}\right]'\| &\leq \left\|\left[\mathbf{B}_c^{0,0}\right]^{-T}\right\|_2\left\|\left[\mathbf{B}_c^{1,0}\right]^T\right\|_2\left\|\hat{\mathbf{U}}_n^{*,c}\right\|+\left\|\left[\mathbf{B}_c^{0,0}\right]^{-T}\right\|_2\|\hat{\mathbf{Z}}_n^*\|\\ &= \left\|\left[\mathbf{B}_c^{0,0}\right]^{-1}\right\|_2\left\|\mathbf{B}_c^{1,0}\right\|_2\left\|\hat{\mathbf{U}}_n^{*,c}\right\|+\left\|\left[\mathbf{B}_c^{0,0}\right]^{-1}\right\|_2\|\hat{\mathbf{Z}}_n^*\|\\ &\leq \frac{n^{\frac{1}{8}}}{\gamma_0}\,\sigma_1\,(\bar{\xi}_1)^{\frac{1}{2}}\,n^{\frac{3}{2}}\left\|\hat{\mathbf{U}}_n^{*,c}\right\|+\frac{n^{\frac{1}{8}}}{\gamma_0}\,\|\hat{\mathbf{Z}}_n^*\|,\end{aligned}$$

so that

$$\|\left[\hat{\mathbf{U}}_n^{*,c}\right]'\|^2\leq\frac{2\,n^{\frac{1}{4}}}{\gamma_0^2}\,\sigma_1^2\,\bar{\xi}_1\,n^3\left\|\hat{\mathbf{U}}_n^{*,c}\right\|^2+\frac{2\,n^{\frac{1}{4}}}{\gamma_0^2}\,\|\hat{\mathbf{Z}}_n^*\|^2.$$

After integrating on $\hat{\Omega}_{1D}$ and leveraging the bound in $(46)_1$, we obtain

$$\|\left[\hat{\mathbf{U}}_n^{*,c}\right]'\|^2_{L^2(\hat{\Omega}_{1D};\mathbb{R}^n)}\leq\frac{2\,n^{\frac{1}{4}}}{\gamma_0^2}\,\sigma_1^2\,\bar{\xi}_1\,n^3\left\|\hat{\mathbf{U}}_n^{*,c}\right\|^2_{L^2(\hat{\Omega}_{1D};\mathbb{R}^n)}+\frac{2\,n^{\frac{1}{4}}}{\gamma_0^2}\,\|\hat{\mathbf{Z}}_n^*\|^2_{L^2(\hat{\Omega}_{1D};\mathbb{R}^n)}$$
$$\leq\left\{\frac{2\,n^{\frac{1}{4}}}{\gamma_0^2}\,\sigma_1^2\,\bar{\xi}_1\,n^3\,\kappa_0(n)+\frac{2\,n^{\frac{1}{4}}}{\gamma_0^2}\right\}\|\hat{\mathbf{Z}}_n^*\|^2_{L^2(\hat{\Omega}_{1D};\mathbb{R}^n)}$$

[3] As an alternative to these steps, one could resort to Young's inequality with the standard choice $\varepsilon=0.5$, combined with the classical Gronwall inequality. This approach would avoid imposing constraints on σ_1, but it would introduce an exponential dependence of $\kappa_0(n)$ on n.

which coincides with result $(46)_2$ where

$$\kappa_1(n) = \frac{2\, n^{\frac{1}{4}}}{\gamma_0^2} \left\{ \sigma_1^2\, \bar{\xi}_1\, n^3\, \kappa_0(n) + 1 \right\}.$$

This leads to result $(43)_2$, after setting $\kappa(n) = \big(\kappa_0(n) + \kappa_1(n)\big)^{\frac{1}{2}}$, namely to (42) with $\beta(n) = \kappa(n)^{-1}$.

Continuity of $\tilde{F}(\cdot)$ We seek a constant $M_F > 0$ such that

$$\big|\tilde{F}(\hat{\mathbf{W}}_m)\big| \leq M_F\, \|\hat{\mathbf{W}}_m\|_{\mathbb{V}_{m,x}} \qquad \forall \hat{\mathbf{W}}_m \in \mathbb{V}_{m,x}. \tag{48}$$

Thanks to the Cauchy-Schwarz inequality and the standard relation between the $L^2(\hat{\Omega}_{1D})$- and the $H^1(\hat{\Omega}_{1D})$-norms, we find

$$\begin{aligned} \big|\tilde{F}(\hat{\mathbf{W}}_m)\big| &= \left| \int_{\hat{\Omega}_{1D}} [\hat{\mathbf{W}}_m]^T\, \hat{\mathbf{F}}_m\, d\hat{x}_1 \right| \leq \int_{\hat{\Omega}_{1D}} \|\hat{\mathbf{W}}_m\|\, \|\hat{\mathbf{F}}_m\|\, d\hat{x}_1 \\ &\leq \|\hat{\mathbf{F}}_m\|_{L^2(\hat{\Omega}_{1D};\,\mathbb{R}^{2m})}\, \|\hat{\mathbf{W}}_m\|_{L^2(\hat{\Omega}_{1D};\,\mathbb{R}^{2m})} \leq \|\hat{\mathbf{F}}_m\|_{L^2(\hat{\Omega}_{1D};\,\mathbb{R}^{2m})}\, \|\hat{\mathbf{W}}_m\|_{\mathbb{V}_{m,x}}, \end{aligned}$$

which coincides with result (48) after identifying M_F with $\|\hat{\mathbf{F}}_m\|_{L^2(\hat{\Omega}_{1D};\,\mathbb{R}^{2m})}$. This constant can be further elaborated to emphasize its dependence on the original source function $\mathbf{f}$, as introduced in (1), and on the chosen modal discretization. In particular, by using the upper bound in (18), the Cauchy-Schwarz inequality and assumption (A1), we can write

$$\begin{aligned} \|\hat{\mathbf{F}}_m\|^2_{L^2(\hat{\Omega}_{1D};\,\mathbb{R}^{2m})} &= \sum_{i=1}^{m} \int_{\hat{\Omega}_{1D}} \sum_{s=1}^{2} \left[\int_{\hat{\gamma}} T_i(\hat{x}_2)\, f_s(\boldsymbol{\Phi}(\hat{\mathbf{z}}))\, j(\hat{\mathbf{z}})\, d\hat{x}_2 \right]^2 d\hat{x}_1 \\ &\leq j_1 \int_{\hat{\Omega}_{1D}} \left[\sum_{i=1}^{m} \|T_i\|^2_{L^2(\hat{\gamma})} \right] \left[\sum_{s=1}^{2} \|f_s(\boldsymbol{\Phi}(\hat{\mathbf{z}}))\, j^{\frac{1}{2}}(\hat{\mathbf{z}})\|^2_{L^2(\hat{\gamma})} \right] d\hat{x}_1 = j_1\, m\, \|\mathbf{f}\|^2_{L^2(\Omega)} \end{aligned}$$

Thus, the continuity constant in (48) can be expressed as $M_F = j_1^{\frac{1}{2}}\, m^{\frac{1}{2}}\, \|\mathbf{f}\|_{L^2(\Omega)}$.

This concludes the proof of the existence and uniqueness of the solution to problem (16). The two stability estimates in (35) follow in a straightforward way from the standard inf-sup analysis [28]. □

Some remarks are in order regarding the main assumptions of Theorem 5. Assumptions (A1) and (A2), which require the orthonormality of the modal basis functions for both velocity and pressure, are consistent with the foundational hypotheses of the HiMod reduction theory (see, e.g., [8, 9]). Assumption (A3), which involves the components of the stiffness matrix associated with the HiMod velocity field, is partially addressed in Remark 1 and can be directly verified when using certain modal families, such as trigonometric functions. Assumption (A4) is constructed so as to prove the inf-sup stability of the bilinear form $\tilde{b}(\cdot,\cdot)$ and is numerically verified in the following section in the case of a trigonometric modal basis. The same section also validates the two conditions on π_1 and σ_1, which essentially impose regularity constraints on the map $\boldsymbol{\Psi}$, namely on the geometry of the physical domain Ω. In addition, the relation between the number of velocity and pressure modal functions represents the

true added value of this theory: not only does it outperform the empirical rule typically adopted in HiMod simulations for Stokes and Navier–Stokes flows (see, e.g., [19, 15, 17]), but it also stems from a rigorous theoretical analysis rather than from a purely practical choice.

Finally, we observe that Theorem 5 enables us to derive error estimates for both the HiMod velocity and pressure, by relying on the classical inf-sup theory [28].

5 Numerical assessment

We aim to support the well-posedness analysis presented in the previous section through numerical experiments, from both a qualitative and quantitative perspective[4]. Particular attention is given to the choice of the modal indices m and n, considering the improvements introduced by Theorem 5 when compared to the selection criteria currently adopted in the state-of-the-art HiMod literature [19, 15, 17].

The second part of the section focuses on the geometric constraints led by the assumptions on π_1 and σ_1, in order to explore the types of domain geometries that are admissible under the proposed theoretical setting.

5.1 Accuracy and efficiency analysis

With a view to performing the numerical assessment, we consider the discrete counterpart of the HiMod formulation introduced in (7) (i.e., in (16)). To this end, we approximate the dynamics along the main direction using a finite element discretization [27]. Clearly, alternative strategies are possible. For instance, in [17], an isogeometric approach is adopted to accurately capture complex centerline geometries in a biomedical context.

We introduce a uniform partition, $\mathcal{T}_h$, of the supporting fiber, with h the constant discretization step, and the associated finite element (FE) space, X_h^r, of the continuous piecewise polynomials of degree r [27]. In accordance with the classical inf-sup theory for the FE discretization of the Stokes problem [28], we adopt an inf-sup stable pair of approximation spaces for the velocity and pressure. Specifically, we employ quadratic piecewise polynomials to model the HiMod velocity and linear piecewise polynomials to define the HiMod pressure. We emphasize that the primary objective of this work is to define a rigorous selection criterion for the modal indices m and n in (5), aimed at properly characterize the spaces V_m and Q_n involved in the HiMod formulation (7). This analysis is carried out independently of the discretization adopted along the x_1-direction.

From an algebraic viewpoint, the discrete counterpart of the HiMod formulation (7) (i.e., (16)) leads to solve a standard saddle point linear system. In more detail, matrix A consists of $2m \times 2m$ square blocks of dimension $N_{h,\mathbf{u}}$, which share the pentadiagonal sparsity pattern typical of a 1D quadratic FE discretization; matrix B is composed by $2m \times n$ rectangular blocks of dimension $N_{h,\mathbf{u}} \times N_{h,p}$, with $N_{h,\mathbf{u}}$ and $N_{h,p}$ the number of the degrees of freedom (DOFs) associated

[4]The simulations are performed on a desktop computer equipped with a 12^{th} Gen Intel® Core™ i7-1260P processor, integrated Mesa Intel® Graphics, and 16 GB of RAM. The computational setup relies on MATLAB and on the package GEOPDEs [30].

with the finite element spaces $[X_h^2]^2$ and X_h^1 involved in the definition of the HiMod velocity and pressure, respectively. We refer to Fig. 1 for some examples of HiMod matrix sparsity pattern when varying the number of modal functions and/or the selected FE discretization.

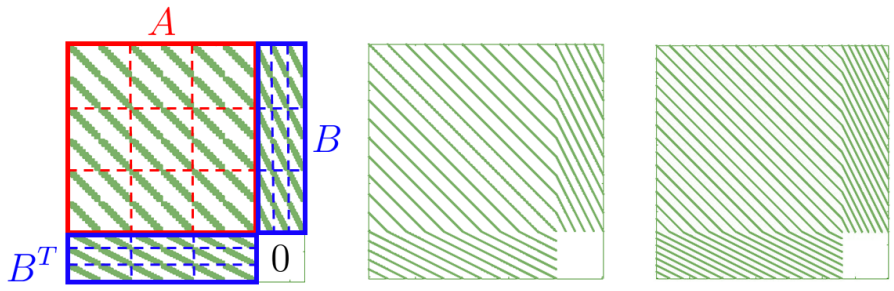

Figure 1: Sparsity pattern of the matrix associated with different HiMod discretization: $m = n = 3$, $N_{h,\mathbf{u}} = 20$, $N_{h,p} = 11$ (left); $m = n = 5$, $N_{h,\mathbf{u}} = 200$, $N_{h,p} = 101$ (middle); $m = n = 7$, $N_{h,\mathbf{u}} = 2000$, $N_{h,p} = 1001$ (right).

In the following, we apply the HiMod discretization to different configurations to investigate the quality and the performance of such a model reduction technique.

5.1.1 Test 1: the rectangular domain

As a first check, we select a basic configuration where Ω coincides with the rectangular domain $(0, L) \times (0, H)$, with $L = 10$ and $H = 1$. Concerning the problem data in (1), we choose $\nu = 0.1$, $\mathbf{f} = \mathbf{0}$, $\mathbf{h}$ the parabolic profile with maximum equal to 1, $\partial\Omega_{\text{in}} = \{0\} \times (0, H)$, $\partial\Omega_{\text{out}} = \{L\} \times (0, H)$ and $\partial\Omega_{\text{lat}} = \partial\Omega \setminus \big(\partial\Omega_{\text{in}} \cup \partial\Omega_{\text{out}}\big)$.
Figure 2, left column displays the colour plot of the reference solution used to verify the HiMod approximation accuracy. It corresponds to a finite element discretization computed using quadratic elements for the velocity and linear elements for the pressure, on a conforming and uniform mesh composed of 45.594 triangles.

The HiMod discretization is carried out by introducing a partition $\mathcal{T}_h$ of the supporting fiber into 100 uniform subintervals, and by employing $m = n = 5$ modal basis functions to represent the transverse dynamics. The middle panel in Fig. 1 displays the sparsity pattern corresponding to this HiMod approximation. The accuracy of the selected HiMod solution is verified by the three panels in Fig. 2, right column that show a highly satisfactory agreement with the corresponding plots of the reference solution. The agreement between the HiMod and FE approximations is also quantitatively confirmed by the values of the relative errors

$$E_p = \frac{\|p^{\text{FE}} - p_n^h\|_{L^2(\Omega)}}{\|p^{\text{FE}}\|_{L^2(\Omega)}} \cdot 100, \qquad E_{\mathbf{u}} = \frac{\|\mathbf{u}^{\text{FE}} - \mathbf{u}_m^h\|_{H^1(\Omega;\mathbb{R}^2)}}{\|\mathbf{u}^{\text{FE}}\|_{H^1(\Omega;\mathbb{R}^2)}} \cdot 100, \tag{49}$$

where $\mathbf{u}^{\text{FE}}$ and p^{FE} are the reference FE velocity and pressure, while $\mathbf{u}_m^h$ and p_n^h denote the corresponding discrete HiMod approximations.

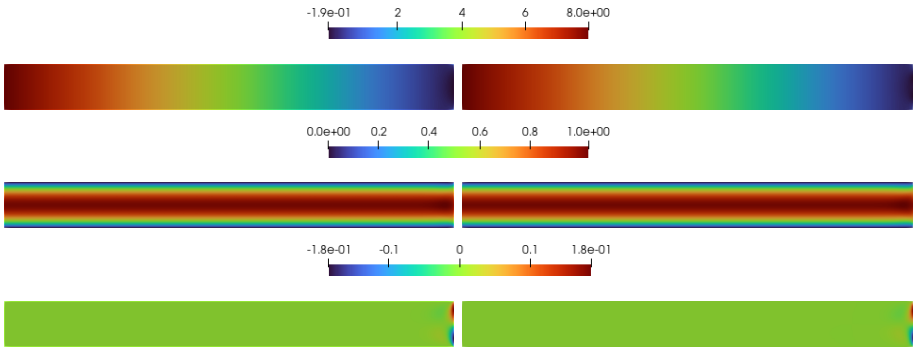

Figure 2: Test 1: reference solution (left) and HiMod approximation (right) with $m = n = 5$, $N_{h,\mathbf{u}} = 200$, $N_{h,p} = 101$ for the pressure (top), the x_1- (middle) and x_2- (bottom) component of the velocity.

Table 1 presents the values of E_p and $E_{\mathbf{u}}$, along with the number of HiMod DOFs, for several combinations of the modal indices m and n, and different FE discretization steps. In particular, we focus on the case $m = n$, as it represents the most cost-effective configuration in terms of DOFs. As expected, the HiMod approximation error decreases as the mesh size h is refined, provided that a sufficiently large number of modes is used. Similarly, increasing the number of modal functions improves the accuracy, as long as h is small enough. We also observe that the error reduction with respect to the number of modes m becomes more pronounced as the mesh is refined, reflecting the high spectral convergence rate of the modal expansion. In particular, a significant improvement in velocity accuracy is observed between $m = 5$ and $m = 9$ for all values of h, confirming that a relatively small number of modes is sufficient to accurately capture the transverse dynamics. Beyond this range, improvements become marginal, suggesting that the remaining error is mainly due to the discretization along the longitudinal direction.

It is of interest to compare the rule currently adopted in the literature for selecting the modal indices, namely $m = n + 2$ [19, 15, 17], with the choice $m = n$ considered in Table 1. In particular, focusing on the block corresponding to $h = 0.125$, we compute the values in (49), denoted by $E_p^{\mathcal{L}}$ and $E_{\mathbf{u}}^{\mathcal{L}}$, by setting $m = n + 2$ for each selected value of n. Table 2 gathers these results together with the error differences

$$\Delta E_p = E_p - E_p^{\mathcal{L}}, \qquad \Delta E_{\mathbf{u}} = E_{\mathbf{u}} - E_{\mathbf{u}}^{\mathcal{L}}.$$

We observe that, for any n, the $m = n$ configuration consistently requires 640 fewer DOFs than the corresponding $\mathcal{L}$ setup, confirming its computational advantage. At the same time, the discrepancies in both pressure and velocity errors remain moderate and tend to decrease as n (and consequently m) increases. This confirms that most of the accuracy is already captured when $m = n$, and the additional modes in the $\mathcal{L}$ configuration bring limited improvements. Hence, the choice $m = n$ appears to be an efficient trade-off, reducing the computational cost while maintaining high accuracy.

As a further verification, we examine the quality of the HiMod approximation when the condition $m \geq n$ on the modal indices in Theorem 5 is violated. We

Table 1: Test 1: quantitative analysis about the accuracy of the HiMod approximation for a different number ($m = n$) of modes (by columns) and values of h (by panels, with $h = 1$, 0.5, 0.25, 0.125, top-bottom).

	$m=5$ $n=5$	$m=9$ $n=9$	$m=13$ $n=13$	$m=17$ $n=17$	$m=21$ $n=21$	$m=25$ $n=25$	$m=29$ $n=29$
E_p	0.44868	0.44179	0.44049	0.44005	0.43986	0.43977	0.43972
$E_{\mathbf{u}}$	4.07944	3.46396	3.34937	3.31687	3.30478	3.29929	3.29661
DOFs	255	459	663	867	1071	1275	1479
E_p	0.27633	0.26056	0.25659	0.25499	0.25422	0.25381	0.25357
$E_{\mathbf{u}}$	3.63625	2.89088	2.74564	2.70410	2.68849	2.68115	2.67730
DOFs	505	909	1313	1717	2121	2525	2929
E_p	0.18211	0.14635	0.13463	0.13379	0.12627	0.12444	0.12332
$E_{\mathbf{u}}$	3.24905	2.22286	1.97278	1.92456	1.85896	1.84093	1.83106
DOFs	1005	1809	2613	3417	4221	4861	5829
E_p	0.16396	0.11761	0.09798	0.08717	0.08045	0.07596	0.07283
$E_{\mathbf{u}}$	3.16239	1.91407	1.51112	1.34059	1.25613	1.20900	1.18011
DOFs	2005	3609	5213	6817	8421	10025	11629

run the HiMod solver with the configurations $m = 5$, $n = 6$ and $m = 5$, $n = 7$, while setting $h = 0.125$ as FE discretization step. It can be checked that, on both cases, the HiMod velocity field still accurately reproduces the reference advective field. Conversely, the pressure remains consistent with the reference one when $m = 5$, $n = 6$, but exhibits a different behavior throughout the channel, along with significant instabilities near the outflow boundary, when $m = 5$, $n = 7$. This is highlighted by the contour lines superimposed on the color plot and by the enlarged views in Fig. 3. This behavior is further supported by the error values E_p and $E_{\mathbf{u}}$ in (49), which remain essentially unchanged for both velocity and pressure when moving from $m = n = 5$ to $m = 5$, $n = 6$, but increase from $E_p = 0.16396$, $E_{\mathbf{u}} = 3.16239$ for $m = n = 5$, to $E_p = 1.76783$, $E_{\mathbf{u}} = 3.71701$ for the choice $m = 5$, $n = 7$.

As a final check in this section, we make some considerations on assumption (A4) underlying Theorem 5. The goal is to provide numerical justification for the exponent assigned to the modal index n in the lower bound. To this end, in the left panel of Fig. 4, we plot with blue markers the minimum eigenvalue of the matrix $\left[\mathbf{B}_c^{0,0}\right]^T \mathbf{B}_c^{0,0}$ as a function of the modal index $m = n$, along with curves corresponding to the function $\gamma_0^2\, n^\mu$ for $\mu = -\frac{1}{4}$, $-\frac{1}{5}$, $-\frac{1}{6}$. Here, the constant $\gamma_0 \in \mathbb{R}^+$ is chosen so that both terms in (A4) match at the smallest eigenvalue, corresponding to $m = n = 1$. It is evident that the choice $\mu = -\frac{1}{4}$ is the one that effectively provides the desired lower bound.

Table 2: Test 1: quantitative analysis about the accuracy of the HiMod approximation for a different number of modes m, n and for $h = 0.125$ (top panel); comparison between the choices $m = n$ and $\mathcal{L}$ (bottom panel).

	$m=7$ $n=5$	$m=11$ $n=9$	$m=15$ $n=13$	$m=19$ $n=17$	$m=23$ $n=21$	$m=27$ $n=25$	$m=31$ $n=29$
$E_p^{\mathcal{L}}$	0.13240	0.10135	0.08883	0.08178	0.07716	0.07391	0.07152
$E_{\mathbf{u}}^{\mathcal{L}}$	2.46781	1.72381	1.44575	1.31672	1.24623	1.20440	1.17713
ΔE_p	0.03156	0.01627	0.00915	0.00540	0.00329	0.00205	0.00131
$\Delta E_{\mathbf{u}}$	0.69459	0.19025	0.06537	0.02386	0.00991	0.00461	0.00298

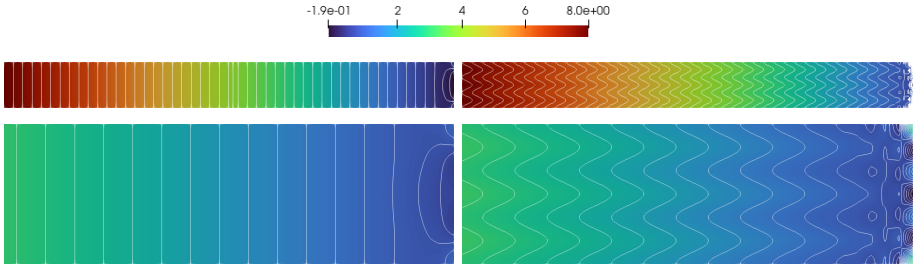

Figure 3: Test 1: HiMod approximation for $m = 5$, $n = 6$, (left) and $m = 5$, $n = 7$ (right), when $N_{h,\mathbf{u}} = 160$, $N_{h,p} = 81$, for the pressure throughout the whole channel (top) and in correspondence with the outflow boundary (bottom).

5.1.2 Test 2: the wavy domain

In this section, we assess the accuracy of the HiMod approach when used to discretize the Stokes problem in a domain featuring a more irregular geometry compared to the simple rectangular case. In particular, the computational domain Ω features a sinusoidal shape with a thickness that decreases from 1 at the inflow $\partial\Omega_{\text{in}}$ to 0.2 at the outflow $\partial\Omega_{\text{out}}$. The supporting fiber Ω_{1D} is also sinusoidal, with an oscillation amplitude of 0.5 and a frequency equal to 2 (see Fig. 5 for a skecth of the domain). The data in (1) are the same as for Test 1, while we assume as reference solution the $\mathbb{P}_2$-$\mathbb{P}_1$ FE discretization associated with a mesh consisting of 152.164 elements.

To efficiently handle the curvature of Ω_{1D} within the HiMod discretization, we adopt the isogeometric variant of this model reduction technique, known as the HIgaMod reduction (Hierarchical IsoGeometric Approach for Model reduction), introduced in [19]. In this approach, the standard finite element discretization along the main flow direction is replaced by isogeometric analysis, which offers a highly flexible and computationally efficient framework for managing complex geometries. More specifically, we partition Ω_{1D} into 1.000 uniform subintervals, employ quadratic and linear splines to approximate the velocity and pressure trends along the main flow direction, respectively and adopt $m = n = 15$ modal functions to capture the transverse dynamics within the reduced model.

Figure 5 compares the reference solution (the two panels in the left column)

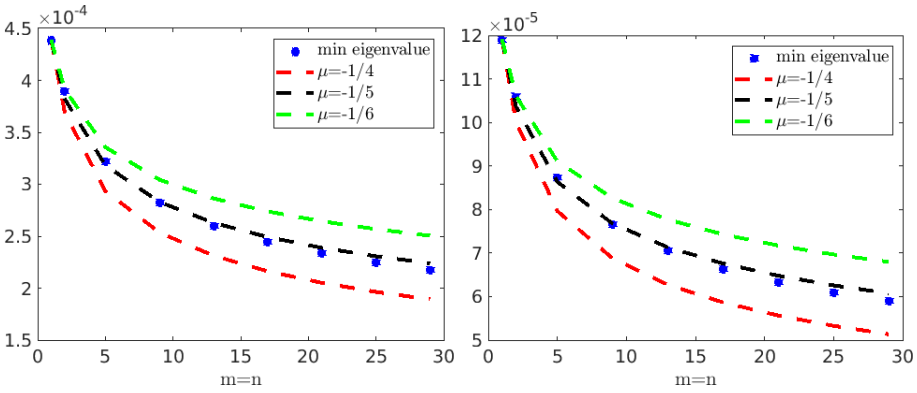

Figure 4: Numerical assessment of assumption (A4) for the rectangular (left) and wavy (right) geometry.

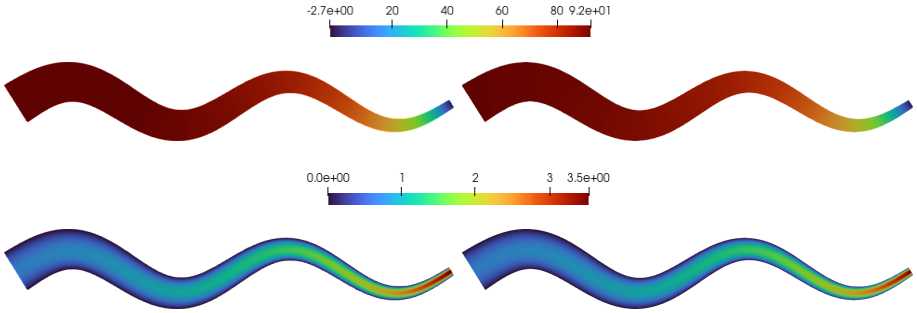

Figure 5: Test 2: reference solution (left) and HiMod approximation (right) with $m = n = 15$, $N_{h,\mathbf{u}} = 2000$, $N_{h,p} = 1001$ for the pressure (top) and the velocity magnitude (bottom).

with the HIgaMod approximation (the two panels in the right column) in terms of pressure (top) and magnitude of the velocity (bottom). The corresponding colour plots show a perfect match between the reference and the reduced solutions, as confirmed by the error values $E_p = 2.77885$ and $E_{\mathbf{u}} = 3.26182$, highlighting the reliability of the proposed approach. The discrepancy in the number of DOFs (384.912 for the reference solution versus 75.015 for the HIgaMod approximation) corroborates the effectiveness of the HIgaMod discretization since significantly reducing the computational complexity.

Finally, we repeat the numerical assessment of assumption (A4) carried out in Fig. 4, left panel for the the wavy geometry. As in the case of the rectangular domain, the choice $\mu = -\frac{1}{4}$ remains the most reasonable for approximating the minimum eigenvalue of the matrix $\left[\mathbf{B}_c^{0,0}\right]^T \mathbf{B}_c^{0,0}$, as highlighted in the right panel of Fig. 4.

5.2 Domain configuration guidelines

The goal of this section is to identify which types of computational domains satisfy the geometric constraints stated in Theorem 5, expressed in terms of the constants π_1 and σ_1 involved in $(19)_3$ and $(20)_2$, respectively. In general,

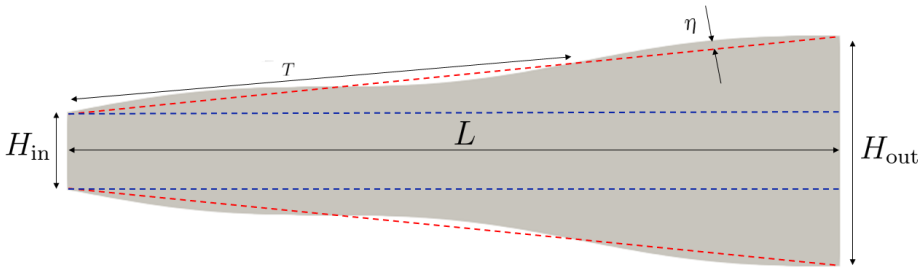

Figure 6: Possible geometric configurations: rectangular (blue), tapered (red), and sinusoidal (grey) domains, along with the associated main defining parameters.

the conditions $\pi_1 = O(m^{-\frac{3}{2}})$ and $\sigma_1 = O(n^{-\frac{3}{2}})$ require these constants to be sufficiently small, which is equivalent to excluding configurations for Ω characterized by abrupt geometric variations either along the horizontal boundaries or the supporting fiber.

A trivial case is represented by rectangular domains, for which both $(19)_3$ and $(20)_2$ hold with $\pi_1 = \sigma_1 = 0$, as $\mathcal{M}_{12}$ and J_{21} vanish identically. In particular, we consider a rectangular domain with length L and height H_{in}, where we assume $L \gg H_{\text{in}}$ consistently with a HiMod setting (see the blue polygon in Fig. 6). We characterize the shape of the rectangle by the quantity H_{in}/L, referred to as the aspect ratio.
Table 3 furnishes the components, J_{gh}, of the Jacobian matrix in (3) for three different values of this ratio, with $g, h = 1, 2$. Specifically, the table lists the maximum value of J_{gh} evaluated at the points in $\mathcal{Z} = \{\mathbf{z}_{\text{eval},ij}\}$, where $\mathbf{z}_{\text{eval},ij} = (x_{1i}^{\text{FE}}, x_{2j}^{\text{Q}})\}$, with x_{1i}^{FE} the FE nodes of the partition $\mathcal{T}_h$ on Ω_{1D} and x_{2j}^{Q} the quadrature nodes along the reference transverse fiber $\hat{\gamma}$, for $i = 1, \ldots, N_{h,\mathbf{u}}$ and $j = 1, \ldots, N_{\text{Q}}$. Notice that the Jacobian components are directly involved in the bound $(20)_2$ and in the definition of the quantity $\mathcal{M}_{12}$, which is upper bounded, up to j, by π_1 in $(19)_3$. Finally, the last two columns provide an estimate of π_1 and σ_1, computed as the maximum over $\mathcal{Z}$ of the left-hand side in $(19)_3$ and $(20)_2$, respectively. The results confirm that the rectangular domain represents the ideal case, being both π_1 and σ_1 equal to zero.

Table 3: Rectangular geometry: values of the components of the Jacobian matrix and of the quantities π_1 and σ_1 for $H_{\text{in}} = 1$ and for different values of the aspect ratio.

H_{in}/L	J_{11}	J_{12}	J_{21}	J_{22}	π_1	σ_1
0.1	0.10000	0	0	1	0	0
0.01	0.01000	0	0	1	0	0
0.001	0.00100	0	0	1	0	0

Now, we explore some geometric perturbations of the rectangular case that still yield acceptable values for π_1 and σ_1. As a first scenario, we modify the

Table 4: Tapered geometry: values of the components of the Jacobian matrix and of the quantities π_1 and σ_1 for $H_{\text{in}} = 1$ (top panel), $H_{\text{in}} = 0.1$ (bottom panel) and for different values of the aspect ratio.

H_{in}/L	J_{11}	J_{12}	J_{21}	J_{22}	π_1	σ_1
0.1	0.10000	0	0.10000	0.99999	0.10000	0.99999
0.01	0.01000	0	0.01000	0.99999	0.01000	0.99999
0.001	0.00100	0	0.00100	0.99999	0.00100	0.99999
0.1	1.00000	0	0.99980	9.99930	0.10000	0.10000
0.01	0.10000	0	0.10000	9.99930	0.01000	0.10000
0.001	0.01000	0	0.01000	9.99930	0.00100	0.10000

domain height at the outflow, which is now taken equal to H_{out}, with $H_{\text{out}} > H_{\text{in}}$. This variation leads to the definition of a tapered geometry (see the red polygon in Fig. 6), which we still characterize using the aspect ratio H_{in}/L. It is worth noting that the tapered geometry gradually converges to the rectangular configuration as H_{out} approaches H_{in}.

Table 4 shows the same values as in Table 3 for two different choices of the domain inflow height, H_{in}. For a fixed value of H_{in}, as expected, both J_{11} and J_{21} lower with decreasing aspect ratio H_{in}/L. Regarding the quantity σ_1, it is useful to recall that it depends on the value of J_{21} and on the determinant in the definition of j. Thus, keeping H_{in} fixed and decreasing the ratio H_{in}/L, we have a reduction in J_{21}, while we can verify that the determinant increases proportionally. As a result, the value of σ_1 remains essentially unchanged. As for π_1, from the definition of $\mathcal{M}_{12}$ in (9) and the left-hand side of $(19)_3$, it turns out that π_1 essentially coincides with the product of σ_1 and J_{11}, since $J_{12} = 0$, as it is confirmed from the values in the table. Finally, a cross-comparison between the two panels in the table reveals that, for a fixed aspect ratio, reducing H_{in} (and consequently L) leads to an increase in J_{11}, J_{21}, and J_{22}, as expected due to the geometric variations. At the same time, σ_1 decreases since the corresponding determinant diminishes when decreasing H_{in}.

The second perturbation of the standard rectangular geometry we consider corresponds to the sinusoidal-shaped domain shown in gray in Fig. 6. This configuration collapses to the tapered geometry as both the oscillation amplitude, η, and frequency, $\phi = T^{-1}$, tend to zero, where T denotes the oscillation period. As a first check, we replicate the same analysis as in Table 4, obtaining the results shown in Table 5. The values of J_{11} and J_{22} are basically the same, as these quantities mainly depend on the aspect ratio of the domain, which is preserved in practice. In contrast, the value of J_{21} scales with the aspect ratio, following a trend similar to the tapered domain. However, unlike the tapered case, where J_{21} remains essentially constant aside from scaling, in the sinusoidal case, it takes on slightly different values due to the oscillation of the horizontal boundaries. This explains the small variations observed in the values of σ_1 and, consequently, in π_1, in relation to the tapered configuration.

Since the sinusoidal geometry depends on a larger set of parameters (i.e., the amplitude and the frequency) compared with the tapered case, we investigate the sensitivity of σ_1 and π_1 with respect to η and ϕ in Table 6 and 7, respectively.
The values of J_{11} and J_{22} remain nearly constant across variations in amplitude and frequency, aligning closely with those observed in the tapered and rectangular domains. Conversely, J_{21} decreases with lower values of either η or ϕ, resulting in a corresponding reduction in both σ_1 and π_1. These quantities progressively converge toward those of the tapered configuration, as shown in Table 4.

Table 5: Sinusodial geometry: values of the components of the Jacobian matrix and of the quantities π_1 and σ_1 for $\eta = 0.01$, $\phi = 1$, $H_{\text{in}} = 1$ (top panel), $H_{\text{in}} = 0.1$ (bottom panel) and for different values of the aspect ratio.

H_{in}/L	J_{11}	J_{12}	J_{21}	J_{22}	π_1	σ_1
0.1	0.10000	0	0.10593	0.99993	0.10594	1.05940
0.01	0.01000	0	0.01063	0.99993	0.01063	1.06268
0.001	0.00100	0	0.00106	0.99993	0.00106	1.06271
0.1	1.00000	0	1.62463	9.99888	0.16248	0.16248
0.01	0.10000	0	0.16279	9.99888	0.01628	0.16281
0.001	0.01000	0	0.01628	9.99888	0.00163	0.16281

Table 6: Sinusodial geometry: values of the components of the Jacobian matrix and of the quantities π_1 and σ_1 for $\phi = 1$, $H_{\text{in}}/L = 0.001$ with $H_{\text{in}} = 1$ (top panel), $H_{\text{in}} = 0.1$ (bottom panel) and for different values of the amplitude.

η	J_{11}	J_{12}	J_{21}	J_{22}	π_1	σ_1
0.1	0.00100	0	0.00163	0.99989	0.00163	1.62812
0.01	0.00100	0	0.00106	0.99993	0.00106	1.06271
0.001	0.00100	0	0.00101	0.99993	0.00101	1.00617
0.01	0.01000	0	0.01628	9.99888	0.00163	0.16281
0.001	0.01000	0	0.01063	9.99927	0.00106	0.10627
0.0001	0.01000	0	0.01006	9.99931	0.00101	0.10062

6 Conclusions

In this work, we have addressed the discretization of the Stokes equations using the HiMod reduction based on the educated modal basis approach previously

Table 7: Sinusodial geometry: values of the components of the Jacobian matrix and of the quantities π_1 and σ_1 for $\eta = 0.001$, $H_{\text{in}}/L = 0.001$ with $H_{\text{in}} = 1$ (top panel), $H_{\text{in}} = 0.01$ (bottom panel) and for different values of the frequency.

ϕ	J_{11}	J_{12}	J_{21}	J_{22}	π_1	σ_1
1	0.00100	0	0.00101	0.99993	0.00101	1.00617
0.1	0.00100	0	0.00100	0.99993	0.00100	1.00052
0.01	0.00100	0	0.00099	0.99993	0.00099	0.99995
1	0.10000	0	0.16279	99.98881	0.00163	0.01628
0.1	0.10000	0	0.10626	99.99270	0.00106	0.01063
0.01	0.10000	0	0.10061	99.99309	0.00101	0.01006

adopted in [11, 15, 17].

The main contribution of this paper is to provide a theoretically grounded discretization strategy for the HiMod framework, improving upon the heuristic criteria currently employed in the literature. In particular, while the use of an inf-sup stable finite element pair for velocity and pressure is a consolidated practice, more care has to be taken in selecting the number of modal functions used to approximate each field. In this regard, existing studies suggest that a stable pressure approximation can be achieved by choosing the number, m, of modal functions for the velocity larger than that, n, for the pressure, following the empirical rule $m = n + 2$.

Theorem 5 formalizes our theoretical contribution by establishing a well-posedness result for the HiMod formulation (7) of the Stokes problem. Under standard hypotheses on the modal bases for velocity and pressure (assumptions (A1) and (A2)), and mild regularity conditions on the spectral behavior of the HiMod stiffness matrix and the coupling matrix between velocity and pressure (assumptions (A3) and (A4)), the inf-sup stability follows. This result is valid provided that the computational domain does not exhibit excessively abrupt geometric variations, either along the horizontal boundaries or the supporting fiber, and that the number of modal functions for the velocity field is chosen greater than or equal to that used for the pressure, namely $m \geq n$. This analysis not only replaces the purely empirical with a theoretically justified selection criterion, but also broadens the spectrum of admissible HiMod discretizations for the Stokes problem (7), thereby extending the current state of the art.

The numerical investigation in Sec. 5 first confirms the accuracy and efficiency of the HiMod approximation under the theoretical assumptions of Theorem 5. It then numerically supports assumption (A4) and assesses the geometric constraints on the domain Ω by evaluating the order of magnitude of the quantities π_1 and σ_1. A particularly insightful check is the test case in Fig. 5, where, despite a violation of the bound on σ_1 (here equal to 6.6891), the HiMod solution still closely matches the reference shown in the figure.

Future research directions include both theoretical and application-oriented developments. From a theoretical perspective, a key objective is to extend the

well-posedness analysis to account also for the discretization along the domain Ω_{1D}. On the practical side, we plan to apply the proposed methodology to realistic engineering problems, such as the simulation of blood flow in patient-specific vascular geometries.

Acknowledgements and funding

This research was conducted within the framework of the European Union's Horizon 2020 research and innovation programme under the Marie Sklodowska-Curie Actions, grant agreement 872442 (ARIA, Accurate Roms for Industrial Applications).
ET acknowledges the INdAM-GNCS Project "Metodi numerici efficienti per problemi accoppiati in sistemi complessi" (CUP E53C24001950001). FB acknowledges the PRIN 2022 PNRR project "ROMEU: Reduced Order Models for Environmental and Urban flows" funded by the European Union – NextGenerationEU under the National Recovery and Resilience Plan (NRRP), Mission 4 Component 2, CUP J53D23015960001.
TC has been supported by MCIN/AEI/10.13039/ 501100011033/ FEDER PID2021-123153OB-C21 grant.

References

[1] F. Chinesta, R. Keunings, A. Leygue, The Proper Generalized Decomposition for Advanced Numerical Simulations, SpringerBriefs in Applied Sciences and Technology, Springer, Cham, 2014.

[2] Y. Maday, Reduced basis method for the rapid and reliable solution of partial differential equations, in: M. Sanz-Solé, J. Soria, J.-L. Varona, J. Verdera (Eds.), International Congress of Mathematicians, Vol. 3, European Mathematical Society, Zürich, 2006, pp. 1255–1270.

[3] J. S. Hesthaven, G. Rozza, B. Stamm, Certified Reduced Basis Methods for Parametrized Partial Differential Equations, SpringerBriefs in Mathematics, Springer, Cham, 2016.

[4] A. Quarteroni, A. Manzoni, F. Negri, Reduced Basis Methods for Partial Differential Equations. An Introduction, UNITEXT, Springer, Cham, 2016.

[5] W. H. Schilders, H. A. van der Vorst, J. Rommes, Model Order Reduction: Theory, Research Aspects and Applications, Mathematics in Industry, Springer, Berlin, Heidelberg, 2008.

[6] P. Benner, S. Gugercin, K. Willcox, A survey of projection-based model reduction methods for parametric dynamical systems, SIAM Rev. 57 (4) (2015) 483–531.

[7] S. Perotto, A survey of Hierarchical Model (Hi-Mod) reduction methods for elliptic problems, in: S. R. Idelsohn (Ed.), Numerical Simulations of Coupled Problems in Engineering, Springer International Publishing, Cham, 2014, pp. 217–241.

[8] A. Ern, S. Perotto, A. Veneziani, Hierarchical model reduction for advection-diffusion-reaction problems, in: K. Kunisch, G. Of, O. Steinbach (Eds.), Numerical Mathematics and Advanced Applications, Springer Berlin Heidelberg, Berlin, Heidelberg, 2008, pp. 703–710.

[9] S. Perotto, A. Ern, A. Veneziani, Hierarchical local model reduction for elliptic problems: a domain decomposition approach, Multiscale Model. Simul. 8 (4) (2010) 1102–1127.

[10] G. G. Gentili, M. Khosronejad, G. Bernasconi, S. Perotto, S. Micheletti, Efficient modeling of multimode guided acoustic wave propagation in deformed pipelines by hierarchical model reduction, Appl. Numer. Math. 173 (2022) 329–344.

[11] M. C. Aletti, S. Perotto, A. Veneziani, HiMod reduction of advection-diffusion-reaction problems with general boundary conditions, J. Sci. Comput. 76 (1) (2018) 89–119.

[12] M. Lupo Pasini, S. Perotto, Hierarchical model reduction driven by a proper orthogonal decomposition for parametrized advection-diffusion-reaction problems, Electron. Trans. Numer. Anal. 55 (2022) 187–212.

[13] M. Lupo Pasini, S. Perotto, Hierarchical model reduction driven by machine learning for parametric advection-diffusion-reaction problems in the presence of noisy data, J. Sci. Comput. 94 (2) (2023) Paper No. 36, 22.

[14] G. Conni, S. Piccardo, S. Perotto, G. M. Porta, M. Icardi, Hiphomε: high-order projection-based homogenization for advection-diffusion-reaction problems, Multiscale Model. Simul. 23 (1) (2025) 640–667.

[15] S. Guzzetti, S. Perotto, A. Veneziani, Hierarchical model reduction for incompressible fluids in pipes, Int. J. Numer. Methods Eng. 114 (5) (2018) 469–500.

[16] S. Perotto, G. Bellini, F. Ballarin, K. Caló, V. Mazzi, U. Morbiducci, Isogeometric Hierarchical Model Reduction for advection-diffusion process simulation in microchannels, Biomechanics of Living Organs, Elsevier, Amsterdam, 2023, Ch. 10, pp. 197–211.

[17] Y. A. Brandes Costa Barbosa, S. Perotto, Hierarchically reduced models for the Stokes problem in patient-specific artery segments, Int. J. Comput. Fluid Dyn. 34 (2) (2020) 160–171.

[18] G. Garcia-Contreras, J. Córcoles, J. A. Ruiz-Cruz, M. Oldoni, G. G. Gentili, S. Micheletti, S. Perotto, Advanced modeling of rectangular waveguide devices with smooth profiles by hierarchical model reduction, IEEE Trans. Microw. Theory Tech. 71 (11) (2023) 4692– 4702.

[19] S. Perotto, A. Reali, P. Rusconi, A. Veneziani, HIGAMod: a hierarchical isogeometric approach for model reduction in curved pipes, Comput. & Fluids 142 (2017) 21–29.

[20] S. Perotto, Hierarchical Model (Hi-Mod) reduction in non-rectilinear domains, in: J. Erhel, M. J. Gander, L. Halpern, G. Pichot, T. Sassi, O. Widlund (Eds.), Domain Decomposition Methods in Science and Engineering XXI, Springer International Publishing, Cham, 2014, pp. 477–485.

[21] S. Perotto, M. G. Carlino, F. Ballarin, Model reduction by separation of variables: A comparison between hierarchical model reduction and proper generalized decomposition, in: S. J. Sherwin, D. Moxey, J. Peiró, P. E. Vincent, C. Schwab (Eds.), Spectral and High Order Methods for Partial Differential Equations ICOSAHOM 2018, Springer International Publishing, Cham, 2020, pp. 61–77.

[22] S. Perotto, A. Veneziani, Coupled model and grid adaptivity in hierarchical reduction of elliptic problems, J. Sci. Comput. 60 (3) (2014) 505–536.

[23] S. Perotto, A. Zilio, Space-time adaptive hierarchical model reduction for parabolic equations, Adv. Model. Simul. Eng. Sci. 2 (1) (2015) 1–45.

[24] S. Perotto, A. Zilio, Hierarchical model reduction: Three different approaches, in: A. Cangiani, R. L. Davidchack, E. Georgoulis, A. N. Gorban, J. Levesley, M. V. Tretyakov (Eds.), Numerical Mathematics and Advanced Applications 2011, Springer Berlin Heidelberg, Berlin, Heidelberg, 2013, pp. 851–859.

[25] P. Blanco, L. M. Álvarez, R. Feijóo, Hybrid element-based approximation for the Navier-Stokes equations in pipe-like domains, Comput. Methods Appl. Mech. Eng. 283 (2015) 971–993.

[26] M. Zancanaro, F. Ballarin, S. Perotto, G. Rozza, Hierarchical model reduction techniques for flow modeling in a parametrized setting, Multiscale Model. Simul. 19 (1) (2021) 267–293.

[27] A. Ern, J.-L. Guermond, Theory and Practice of Finite Elements, Applied Mathematical Sciences, Springer, New York, 2004.

[28] D. Boffi, F. Brezzi, M. Fortin, Mixed Finite Element Methods and Applications, Vol. 44 of Springer Series in Computational Mathematics, Springer, Berlin, Heidelberg, 2013.

[29] C. Canuto, M. Y. Hussaini, A. Quarteroni, T. A. Zang, Spectral methods. Fundamentals in Single Domains, Scientific Computation, Springer, Berlin, Heidelberg, 2006.

[30] C. de Falco, A. Reali, R. Vázquez, GeoPDEs: A research tool for isogeometric analysis of PDEs, Adv. Eng. Softw. 42 (3) (2011) 1020–1034.

MOX Technical Reports, last issues

Dipartimento di Matematica
Politecnico di Milano, Via Bonardi 9 - 20133 Milano (Italy)

47/2025 Gimenez Zapiola, A.; Consolo, A.; Amaldi, E.; Vantini, S.
Penalised Optimal Soft Trees for Functional Data

46/2025 Mirabella, S.; David, E.; Antona, A.; Stanghellini, C.; Ferro, N.; Matteucci, M.; Heuvelink, E.; Perotto, S.
On the Impact of Light Spectrum on Lettuce Biophysics: A Dynamic Growth Model for Vertical Farming

45/2025 Caliò, G.; Ragazzi, F.; Popoli, A.; Cristofolini, A.; Valdettaro, L; De Falco, C.; Barbante, F.
Hierarchical Multiscale Modeling of Positive Corona Discharges

44/2025 Brivio, S.; Fresca, S.; Manzoni, A.
Handling geometrical variability in nonlinear reduced order modeling through Continuous Geometry-Aware DL-ROM

43/2025 Tomasetto, M.; Manzoni, A.; Braghin, F.
Real-time optimal control of high-dimensional parametrized systems by deep-learning based reduced order models

41/2025 Torzoni, M.; Maisto, D.; Manzoni, A.; Donnarumma, F.; Pezzulo, G.; Corigliano, A.
Active digital twins via active inference

42/2025 Franco, N. R.; Manzoni, A.; Zunino, P.; Hesthaven, J. S.
Deep orthogonal decomposition: a continuously adaptive neural network approach to model order reduction of parametrized partial differential equations

40/2025 Tentori, C.A.; Gregorio, C.; ...; Ieva, F.; Della Porta, M.G.
Clinical and Genomic-Based Decision Support System to Define the Optimal Timing of Allogeneic Hematopoietic Stem-Cell Transplantation in Patients With Myelodysplastic Syndromes

37/2025 Spreafico, M.; Ieva, F.; Fiocco, M.
Causal effect of chemotherapy received dose intensity on survival outcome: a retrospective study in osteosarcoma

Gimenez Zapiola, A.; Boselli, A.; Menafoglio, A.; Vantini, S.
Hyper-spectral Unmixing algorithms for remote compositional surface mapping: a review of the state of the art